https://doi.org/10.5194/acp-2021-395
Preprint. Discussion started: 1 June 2021

Atmospheric Chemistry and Physics Discussions
Open Access
EGU

Weakening of Antarctic Stratospheric Planetary Wave Activities in Early Austral Spring Since the Early 2000s: A Response to Sea Surface Temperature Trends

YIHANG HU, WENSHOU TIAN, JIANKAI ZHANG, TAO WANG, MIAN XU

Key Laboratory for Semi-Arid Climate Change of the Ministry of Education, College of Atmospheric Sciences, Lanzhou University, China

*Correspondence to: wstian@lzu.edu.cn

https://doi.org/10.5194/acp-2021-395
Preprint. Discussion started: 1 June 2021

Atmospheric Chemistry and Physics Discussions
Open Access
EGU

Abstract

Using multiple reanalysis datasets and modeling simulations, the trends of Antarctic stratospheric planetary wave activities in early austral spring since the early 2000s are investigated in this study. We find that the stratospheric planetary wave activities in September have weakened significantly since 2000, which is related to the weakening of the tropospheric wave sources in the extratropical southern hemisphere. Further analysis indicates that the trend of September sea surface temperature (SST) over 20°N-70°S is statistically linked to the weakening of stratospheric planetary wave activities. Numerical simulations support the result that the SST trend in the extratropical southern hemisphere (20°S-70°S) and the tropics (20°N-20°S) induce the weakening of wave-1 component of tropospheric geopotential height in the extratropical southern hemisphere, which subsequently leads to the decrease in stratospheric wave flux. The responses of stratospheric wave activities in the southern hemisphere to stratospheric ozone recovery is not significant in simulations. In addition, both reanalysis data and numerical simulations indicate that the Brewer-Dobson circulation (BDC) related to wave activities in the stratosphere has also been weakening in early austral spring since 2000 due to the trend of September SST in the tropics and extratropical southern hemisphere.

Key words: *Antarctic; Stratospheric planetary wave activities; Tropospheric wave sources; Sea surface temperature*

https://doi.org/10.5194/acp-2021-395
Preprint. Discussion started: 1 June 2021

Atmospheric Chemistry and Physics Discussions
Open Access
EGU

1. Introduction

The stratospheric planetary wave activities have important influences on stratospheric temperature (e.g., Hu & Fu, 2009; Lin et al., 2009; Li & Tian, 2017; Li et al., 2018), polar vortex (e.g., Kim et al., 2014; Zhang et al., 2016; Hu et al., 2018) and distribution of chemical substances (e.g., Gabriel et al., 2011; Ialongo et al., 2012; Kravchenko et al., 2011; Zhang et al., 2019a). Meanwhile, the stratospheric circulation modulated by planetary waves can exert impacts on tropospheric weather and climate (e.g., Haigh et al., 2005; Zhang et al., 2019b) through downward control processes (Haynes et al., 1991), which is useful for extended forecast by using preceding signals in the stratosphere (e.g., Baldwin et al., 2001; Wang et al., 2020).

The planetary perturbations generated by large-scale topography, convection and continent-ocean heating contrast can propagate from the troposphere to the stratosphere (Charney & Drazin, 1961) and form stratospheric planetary waves. As the land-sea thermal contrast in the northern hemisphere is larger than that in the southern hemisphere and produces stronger zonal forcing for the genesis of stratospheric waves, the majority of attention has been given to wave activities and their impacts on weather and climate in the northern hemisphere (e.g., Kim et al., 2014; Zhang et al., 2016; Hu et al., 2018). However, planetary wave activities in the southern hemisphere also play an important role in heating the stratosphere dynamically (e.g., Hu & Fu, 2009; Lin et al., 2009), which suppresses Polar Stratospheric Clouds (PSCs) formation and ozone depletion (e.g., Shen et al., 2020a; Tian et al., 2018). The Antarctic sudden stratospheric warming (SSW) that occurred in 2002 (e.g., Baldwin et al., 2003; Nishii & Nakamura, 2004; Newman & Nash, 2005) and 2019 (e.g., Yamazaki el al., 2020; Shen et al., 2020a; Shen et al., 2020b) were associated with significant upward propagation of wave flux. Such episodes are extraordinarily rare in the history, and the one in 2019 contributed to the formation of the smallest Antarctic ozone hole on record (WMO, 2019). In addition, some studies reported that wildfires in Australia at the end of 2019 are related to negative phase of the Southern Annular Mode (SAM), which was induced by the extended influence of the SSW event that occurred in September (Lim et al., 2019; Shen et al., 2020b). In a word, the Antarctic planetary wave activities are important for the stratosphere-troposphere interactions and climate system in the southern hemisphere.

Long-term observations in the Antarctic stratosphere show a significant ozone decline from the early 1980s to the early 2000s due to anthropogenic emission of chlorofluorocarbons (CFCs) (WMO, 2011) and a recovery signal since 2000s because of phasing out CFCs in response to Montreal Protocal (e.g., Angell and Free, 2009; Krzyścin, 2012; Zhang et al., 2014; Banerjee et al., 2020). The Antarctic stratospheric ozone depletion and recovery have important impacts on climate in the southern hemisphere. The ozone depletion cools the Antarctic stratosphere through reducing absorption of radiation and leads to the strengthening of Antarctic polar vortex during austral spring (e.g., Randel & Wu, 1999; Solomon et al., 1999; Thompson et al., 2011). The anomalous circulation in the Antarctic stratosphere during austral spring exerts impacts on tropospheric circulations (e.g., intensification of SAM index, poleward shift of tropospheric jet position and expansion of the Hadley cell edge) in the subsequent months (e.g., Thompson et al., 2011; Swart & Fyfe, 2012; Son et al., 2018; Banerjee et

https://doi.org/10.5194/acp-2021-395
Preprint. Discussion started: 1 June 2021

al., 2020) and influences the distribution of precipitation and dry zone in the southern hemisphere (e.g., Thompson et al., 2011; Barnes et al., 2013; Kang et al., 2011). Following the healing of ozone loss in the Antarctic ozone hole since 2000s (e.g., Solomon et al., 2016; Susan et al., 2019), great attention has been paid on possible impacts of ozone recovery on climate system in the southern hemisphere (e.g., Son et al., 2008; Barnes et al., 2013; Xia et al., 2020; Banerjee et al., 2020). Son et al. (2008) implemented the Chemistry-Climate Model Validation (CCMVal) models to predict the response of the southern hemisphere westerly jet to stratospheric ozone recovery. Based on the Phase 5 of Coupled Model Intercomparison Projects (CMIP5) models, Barnes et al. (2013) proposed that the tropospheric jet and dry zone edge no longer shift poleward during austral summer since the early 2000s due to ozone recovery. Banerjee et al. (2020) analyzed observations and reanalysis datasets. They found that following the ozone recovery after 2000, the increase of SAM index and the poleward shifting of tropospheric jet position as well as the Hadley cell edge all experienced a pause. Their results suggest that ozone depletion and recovery have made important contributions to the climate shift that occurred around 2000 in the southern hemisphere.

However, some previous studies have reported zonally asymmetric warming patterns in Antarctic stratosphere, which are generated by increased planetary wave activities during austral spring from the early 1980s to the early 2000s (Hu & Fu, 2009; Lin et al., 2009). Note that the Antarctic stratosphere was experiencing radiative cooling in the same period due to ozone depletion (e.g., Randel & Wu, 1999; Solomon et al., 1999; Thompson et al., 2011). The increase in stratospheric planetary wave activities

https://doi.org/10.5194/acp-2021-395
Preprint. Discussion started: 1 June 2021

cannot be explained by ozone decline, because the acceleration of stratospheric circumpolar wind caused by radiative cooling induces more wave energy to be reflected back to the troposphere (e.g., Andrews et al., 1987; Holton et al., 2004). Hu & Fu (2009) attributed the increase in Antarctic stratospheric wave activities to the SST trend from the 1980s to the 2000s. Their results indicate that in addition to ozone change, other factors such as SST trend also contribute to climate change in the southern hemisphere. Moreover, the phase of Interdecadal Pacific Oscillation (IPO) also changed at around 2000 (e.g., Trenberth et al., 2013). SST variation influences Rossby wave propagation and tropospheric wave sources, and thereby indirectly affects stratospheric wave activities (e.g., Lin et al., 2012; Hu et al., 2018; Tian et al., 2018). The questions here are: (1) Has the stratospheric planetary wave activity trend in the southern hemisphere been shifting since the 2000s? (2) What are the factors responsible for the trend of Antarctic stratospheric planetary wave activity since the 2000s?

In this study, we reveal the trend of Antarctic planetary wave activity in early austral spring since the 2000s based on multiple reanalysis datasets. We also conduct sensitive experiments forced by linear increments of ozone and SST fields since the 2000s to investigate the response of Antarctic planetary activity to above two factors. The remainder of the paper is organized as follows. Section 2 describes the data, methods and configurations of model simulations. Section 3 presents the trends of stratospheric and tropospheric wave activities in early austral spring. Section 4 investigates the connections between the trends of SST and stratospheric wave activities. Sections 5 discusses the responses of tropospheric wave source and stratospheric wave

https://doi.org/10.5194/acp-2021-395
Preprint. Discussion started: 1 June 2021

activity to SST trend based on simulations. Major conclusions and discussion are presented in Section 6.

2. Datasets, methods and experimental configurations

a. Datasets

In this study, daily and monthly mean data extracted from the Modern-Era Retrospective analysis for Research and Applications Version 2 (MERRA-2; Bosilovich et al., 2015) dataset are used to calculate trends of zonally averaged zonal wind and temperature, BDC, tropospheric wave sources, and the Elisassen-Palm (E-P) flux and its divergence in September. To verify the trend of stratospheric E-P flux, we also refer to the results derived from the European Centre for Medium-range Weather Forecasting (ECMWF) Interim Reanalysis (ERA-Interim; Dee et al., 2011) dataset, the Japanese 55-year Reanalysis (JRA-55; Kobayashi et al., 2015) dataset and the National Centers for Environmental Prediction-Department of Energy Global Reanalysis 2 (NCEP-2; Kanamitsu et al., 2002) dataset.

SST data are extracted from the Extended Reconstructed Sea Surface Temperature (ERSST) dataset, which is a global monthly mean sea surface temperature dataset derived from the International Comprehensive Ocean-Atmosphere Dataset (ICOADS). The ERSST is on global 2°×2° grid and covers the period from January 1854 to the present. We use the newest version (version 5, i.e., v5) dataset to calculate trends and correlations, and produce SST forcing field for model simulations. More details about this version of ERSST can be found in Huang et al. (2017).

In addition, the unfiltered Interdecadal Pacific Oscillation (IPO) index derived

https://doi.org/10.5194/acp-2021-395
Preprint. Discussion started: 1 June 2021

Atmospheric Chemistry and Physics Discussions

from the ERSST v5 dataset is also used in this study. The IPO index is available at https://psl.noaa.gov/data/timeseries/IPOTPI/tpi.timeseries.ersstv5.data and more detailed information about the index can be found in Henley et al. (2015).

b. Diagnosis of wave activities and Brewer-Dobson circulation

Planetary wave activities are measured by E-P flux ($\vec{F} \equiv (0, F^{(\phi)}, F^{(z)})$) and its divergence D_F. Their algorithms are expressed by Eqs. (1)-(3) (Andrews et al., 1987):

$$F^{(\phi)} = \rho_0 a \cos\phi(\overline{u_z}\,\overline{v'\theta'} / \overline{\theta}_z - \overline{v'u'}) \tag{1}$$

$$F^{(z)} = \rho_0 a \cos\phi\{[f - (a\cos\phi)^{-1}(\overline{u}\cos\phi)_\phi]\overline{v'\theta'} / \overline{\theta}_z - \overline{w'u'}\} \tag{2}$$

$$D_F = \frac{\nabla \cdot \vec{F}}{\rho_0 a \cos\phi} = \frac{(a\cos\phi)^{-1}\frac{\partial}{\partial\phi}(F^{(\phi)}\cos\phi) + \frac{\partial F^{(z)}}{\partial z}}{\rho_0 a \cos\phi} \tag{3}$$

where u, v represent zonal and meridional components of horizontal wind, w is vertical velocity, θ is potential temperature, a is the Earth radius, f is the Coriolis parameter, z is geopotential height, ϕ is latitude, ρ_0 is the background air density.

The quasi-geostrophic refractive index (RI) is used to diagnose the environment of wave propagation (Chen & Robinson, 1992). Its algorithm is written as Equation (4):

$$RI = \frac{\overline{q}_\varphi}{\overline{u}} - \left(\frac{k}{a\cos\varphi}\right)^2 - \left(\frac{f}{2NH}\right)^2 \tag{4}$$

where the zonal-mean potential vorticity meridional gradient $\overline{q}_\varphi$ is

$$\overline{q}_\varphi = \frac{2\Omega}{a}\cos\varphi - \frac{1}{a^2}\left[\frac{(\overline{u}\cos\varphi)_\varphi}{a\cos\varphi}\right]_\varphi - \frac{f^2}{\rho_0}\left(\rho_0\frac{\overline{u}_z}{N^2}\right)_z \tag{5}$$

q, k, N^2 and Ω are the potential vorticity, zonal wave number, buoyancy frequency, and Earth's angular frequency, respectively.

The Brewer-Dobson circulation driven by wave breaking in the stratopause is closely related to stratospheric wave activities. Its meridional and vertical components

https://doi.org/10.5194/acp-2021-395
Preprint. Discussion started: 1 June 2021

$(\bar{v}^*, \bar{w}^*)$ and stream function ($\psi^*(p,\phi)$) are expressed by Eqs. (4)-(6) (Andrews et al., 1987; Birner & Bönisch, 2011) :

$$\bar{v}^* \equiv \bar{v} - \rho_0^{-1}(\rho_0 \overline{v'\theta'} / \bar{\theta}_z)_z \quad (6)$$

$$\bar{w}^* \equiv \bar{w} + (a\cos\phi)^{-1}(\cos\phi \cdot \overline{v'\theta'} / \bar{\theta}_z)_\phi \quad (7)$$

$$\psi^*(p,\phi) = \int_0^p \frac{-2\pi a \cdot \cos\phi \cdot \bar{v}^*(p'',\phi)}{g} dp'' \quad (8)$$

where p is the air pressure, π is the circular constant, g is the gravitational acceleration.

In Eqs. (1)-(8), the overbar and prime denote zonal mean and departure from zonal mean, respectively. The subscripts denote partial derivatives. The Fourier decomposition is used to obtain components of Eqs. (1)-(3) with different zonal wave numbers. Meanwhile, the Fourier decomposed components of geopotential height zonal deviations are also used to determine tropospheric wave sources.

c. Statistical methods

The trend is measured by the slope of linear regression based on the least square estimation. The correlation is used to analyze statistical links between different variables. In this paper, all the time series have been linearly detrended before calculating correlation coefficients (r) and their corresponding significances.

The change-point testing (e.g. Banerjee et al., 2020) is used to make sure the significance of trend or correlation coefficient is not unduly influenced by some particular beginning or ending years, and thereby confirm that the trend exists objectively.

We use two-tailed student's t test to calculate the significances of trend, correlation

https://doi.org/10.5194/acp-2021-395
Preprint. Discussion started: 1 June 2021

coefficient or mean difference. The result of significance test is measured by p value or confidence intervals in this paper. $p \leq 0.1$, $p \leq 0.05$ and $p \leq 0.01$ suggest the trend, correlation coefficient or mean difference is significant at/above the 90%, 95% and 99% confidence levels, respectively. The confidence interval of trend is shown in (7):

$$[\hat{b} - t_{1-\alpha/2}(n-2)\hat{\sigma}_b, \hat{b} + t_{1-\alpha/2}(n-2)\hat{\sigma}_b] \tag{7}$$

where $\hat{b}$ is estimated value of slope, $\hat{\sigma}_b$ is standard error of slope and it is written as: $\hat{\sigma}_b = \hat{b} \cdot \sqrt{\frac{\frac{1}{r^2} - 1}{n-2}}$, $t_{1-\alpha/2}(n-2)$ denotes the value of t-distribution with the degree of freedom equal to $n-2$ and the two-tailed confidence level equal to $1-\alpha$ ($\alpha = 0.90$, 0.95 or 0.99). The confidence interval of mean difference is expressed by Eq. (8):

$$[\bar{X} - \bar{Y} - t_{1-\alpha/2}(M+N-2) \cdot S_w \cdot \sqrt{\frac{1}{M} + \frac{1}{N}}, \bar{X} - \bar{Y} + t_{1-\alpha/2}(M+N-2) \cdot S_w \cdot \sqrt{\frac{1}{M} + \frac{1}{N}}] \tag{8}$$

where

$$S_w = \sqrt{\frac{1}{M+N-2}[\sum_{i=1}^{M}(X_i - \bar{X})^2 + \sum_{j=1}^{N}(Y_j - \bar{Y})^2]} \tag{9}$$

Here, $\bar{X}$ and $\bar{Y}$ are the sample averages, M and N are the numbers of sample sizes with two populations, $t_{1-\alpha/2}(M+N-2)$ denotes the value of t-distribution with the degree of freedom equal to $M+N-2$ and the two-tailed confidence level equal to $1-\alpha$.

Previous studies have indicated that SST impact on the stratosphere shows a spatial dependence (e.g. Xie et al., 2020). To find out a robust relationship between the trend of SST in a specific region and the trend of stratospheric wave activities, we divide

https://doi.org/10.5194/acp-2021-395
Preprint. Discussion started: 1 June 2021

the global ocean into three regions: SH (the extratropical southern hemisphere, 70°S-20°S), TROP (the tropics, 20°S-20°N) and NH (the extratropical northern hemisphere, 20°N-70°N). Since the impacts in different regions might be combined, we also consider three combined regions named as SHtrop (the extratropical southern hemisphere and the tropics, 70°S-20°N), NHtrop (the extratropical northern hemisphere and the tropics, 20°S-70°N) and the Globe (70°S-70°N). To find statistical connections between the trend of SST and that of stratospheric wave activities, we examine the first three leading patterns (EOF1, EOF2, EOF3) and principal components (PC1, PC2, PC3) of SST in above six regions obtained from Empirical Orthogonal Function (EOF) analysis. In all the six regions, there is always one EOF modes that shows great similarity to the spatial pattern of trend (not shown) as we do not detrend SST time series when the EOF analysis is carried out. Thus, the significance of the correlation between the PC time series of that EOF mode and time series of stratospheric E-P flux can be used as the criterion to determine the statistical connection between the trend of SST and the trend of stratospheric wave activities.

d. The model and experiment configurations

The FWSC component in the Community Earth System Model (CESM; version 1.2.0) is used to verify the impact of SST and ozone recovery trends on tropospheric wave sources and stratospheric wave activities in early austral spring. The FWSC component is the Whole Atmosphere Community Climate Model version 4 (WACCM4) with specified chemistry forcing fields (such as ozone, greenhouse gases (GHG), aerosols and so on), which have fixed values in 2000 by default. The WACCM4

https://doi.org/10.5194/acp-2021-395
Preprint. Discussion started: 1 June 2021

includes active atmosphere, data ocean (run as a prescribed component, simply reading SST forcing data instead of running ocean model), land and sea ice. Important physics schemes in the WACCM4 are based on those in the Community Atmospheric Model version 4 (CAM4; Neale et al., 2013). The WACCM4 uses a finite-volume dynamic framework and extends from the ground to approximately 145 km (5.1×10^{-6} hPa) altitude in the vertical with 66 vertical levels. The simulations presented in this paper are conducted at a horizontal resolution of 1.9°×2.5°. More information about the WACCM can be found in Marsh et al. (2013).

Control experiments and sensitive experiments are conducted to investigate responses of Antarctic stratospheric wave activities to SST trend and the ozone recovery trend in early austral spring. For the experiments of SST trends, monthly mean global SST during 1980-2000 derived from the ERSST v5 dataset is used as SST forcing field in the control experiment (sstctrl). For the four sensitive experiments (sstNH, sstSH, ssttrop, sstSHtrop), linear increments of SST in different regions in September during 2000-2017 are used as the forcing field. Ozone, aerosols and greenhouse gases (GHG) in the control experiment and the four sensitive experiments all have the fixed values in 2000. For the experiments of ozone recovery trend, monthly mean three-dimensional global ozone during 1980-2000 derived from the MERRA-2 dataset is used as the ozone forcing field in the control experiment (O3ctrl). The sensitive experiment (O3sen) is forced by linear increments of ozone in September during 2001-2017. The SSTs in O3ctrl and O3sen both are monthly mean global SST during 1980-2000. The aerosol and greenhouse gases values in 2000 are used. These experiment configurations are

https://doi.org/10.5194/acp-2021-395
Preprint. Discussion started: 1 June 2021

summarized and listed in Table 1 and Table 2.

First, we run the FWSC component to generate randomly different initial conditions for 120 years with free run. Then, each experiment includes 100 ensemble members that run from July to September forced by these initial conditions from the 21st year to the 120th year in July. The forcing fields of SST and ozone are only superposed from July to September. July and August are taken as spin-up time and simulations during this period are discarded. The ensemble mean in September derived from these 100 ensemble members is regarded as the final result of each experiment. A similar approach is implemented for sensitive experiments, in which the forcing fields superposed only in certain months. The same approach has been used in previous studies (e.g., Zhang et al., 2018).

3. Trend of planetary wave activities in early austral spring

Figure 1 shows the trends of stratospheric planetary wave activities in the southern hemisphere September during 1980-2000 and 2000-2017, respectively. Note that the vertical E-P flux entering into the stratosphere over 50°S-70°S in September has been increasing during 1980-2000, accompanied by intensified wave flux convergence in the upper stratosphere (Fig. 1a) that is mainly contributed by the wave-1 component (Fig. 1b). This feature implies that the stratospheric planetary wave activities have strengthened in early austral spring during 1980-2000. A similar result has been reported in previous studies (Hu & Fu, 2009; Lin et al., 2009). During 2000-2017, however, vertical transport of stratospheric E-P flux weakened over the subpolar region of the southern hemisphere, which was accompanied by intensified wave flux

https://doi.org/10.5194/acp-2021-395
Preprint. Discussion started: 1 June 2021

divergence in the upper stratosphere (Fig. 1d) mainly contributed by the wave-1 component (Fig. 1e) while the wave-2 component also made certain contributions (Fig. 1f). Similar features also appear in August, but not as significant as that in September (Fig. S1). For this reason, hereafter we focus on the features in September.

The SSW that occurred in 2002 was accompanied with large upward wave fluxes in the stratosphere, which is extremely rare in history and has been studied in numerous previous studies (e.g., Baldwin et al., 2003; Nishii & Nakamura, 2004; Newman & Nash, 2005). Since the period with a negative trend of stratospheric vertical wave flux is short, it is necessary to further investigate whether such a negative trend is artificially influenced by the single year of 2002. Therefore, following Banerjee et al. (2020), we use a change-point method to test the significance of the trend during various periods based on four reanalysis datasets (ERA-Interim, MERRA-2, JRA-55, NCEP-2). Figures 2a (including the year 2002) and 2b (excluding the year 2002) display the time series (Fz) of area-weighted vertical stratospheric wave flux over the southern hemisphere subpolar region obtained from different reanalysis datasets. Note that the wave flux time series obtained from the four reanalysis datasets all present a positive trend from the early 1980s to the early 2000s and a negative trend from the early 2000s to present, regardless of whether the extreme value in 2002 is removed or not. The correlation coefficients of the time series between these reanalysis datasets are above 0.9 and statistically significant (Table 3), suggesting that the time series derived from different datasets are consistent with each other. Figures 2c-f show the trends and corresponding confidence intervals calculated with four different beginning years (1980,

https://doi.org/10.5194/acp-2021-395
Preprint. Discussion started: 1 June 2021

1981, 1982, 1983), four different ending years (2015, 2016, 2017, 2018), and change-point years from 1998 to 2013. The trends and confidence intervals in Figures 2g-j are the same as that in Figures 2c-f, except that the extreme value in 2002 is removed. The positive trend from the early 1980s to the 21st century remains significant regardless of different beginning years and ending change-point years (Figs. 2c-j). However, Figures 2c-f and Figures 2g-j indicate that the positive value of the trend is decreasing gradually when the period is prolonged, which is apparently attributed to the negative trend with the beginning change-point year of around 2000. Although the negative trend from the change-point year to ending year becomes less significant when the value in 2002 is removed, it remains significant in some periods, which are also illustrated on diagrams of latitude-pressure profiles (Fig. S2). Therefore, the weakening of stratospheric wave activities in early austral spring since the early 2000s is robust. In this paper, we take the year 2000 as the beginning year of the weakening trend to simplify descriptions in the following discussion.

Figure 3 shows the trends of tropospheric wave sources in September since 2000. There is a significant positive trend of the wave-1 component in 500 hPa geopotential height over the southern Indian ocean and a significant negative trend over the southern Pacific, which form an out-of-phase superposition on its climatology (Fig. 3b). The trend pattern of wave-2 component is also out-of-phase with its climatology, although it is not significant (Fig. 3c). The above features still maintain when the values in 2002 are removed (Fig. S3b, c), implying that the southern hemispheric tropospheric wave sources in early austral spring have weakened since 2000, which is also reflected in the

https://doi.org/10.5194/acp-2021-395
Preprint. Discussion started: 1 June 2021

decrease of tropospheric vertical wave flux (Fig. 3d, e; Fig. S3d, e).

4. Role of SST trends in the weakening of Antarctic stratospheric wave activities

In this section, we further explore factors that lead to the weakening of tropospheric wave sources and stratospheric wave activities since the early 2000s in early austral spring. Numerous studies reported that the variations in sea surface temperature can affect stratospheric climate (e.g., Li, 2009; Hurwitz et al., 2011; Lin et al., 2012; Hu et al., 2014; Hu et al., 2018; Tian et al., 2018; Xie et al., 2020). Hu & Fu (2009) also attributed the strengthened stratospheric wave activities in the southern hemisphere to SST trend from the early 1980s to the early 2000s. Furthermore, global SST in September during 2000-2017 also has a significant trend. The significant warming pattern is mainly found over the southern Indian ocean, the southern Atlantic ocean, the eastern and western equatorial Pacific, the western equatorial and Northern Atlantic ocean (Fig. 4b). A significant cooling pattern is located over the southeast Pacific (Fig. 4b). In a word, the spatial pattern of SST trend during 2000-2017 is obviously different from that during 1980-2000 (Fig. 4a, b). Thus, it is necessary to analyze the connection between SST trend and wave activity trend since the early 2000s.

Figure 5 shows the significance of principle component (PC) trends (Figs. 5a-f) of SST in different regions, and the significance of correlations (Figs. 5g-l) between the PC time series and Fz during various periods in September. The trend of PC1 time series in SH region is significant during serval periods (Fig. 5a), while the correlation between PC1 and Fz is only significant with the particular ending year of 2015 (Fig. 5g). This

https://doi.org/10.5194/acp-2021-395
Preprint. Discussion started: 1 June 2021

feature suggests that the connection between the SST trend in SH region and the trend of stratospheric wave activity is not robust. The correlation between trend of stratospheric wave activity and that of SST in TROP or NH region is also weak (Fig. 5e, f). As for the combined regions, note that the PC2 time series in SHtrop region has a significant trend (Fig. 5d) and the correlation between the PC2 time series in SHtrop and Fz with the beginning year of around 2000 is also significant (Fig. 5j) regardless of different ending years. This feature implies that the extratropical southern hemisphere and tropical SST has a robust connection with stratospheric wave activities in early austral spring since the early 2000s. The correlations between Fz and all PC time series in NHtrop (Fig. 5k) and Globe (Fig. 5l) region are not as robust as that between Fz and PC2 time series in SHtrop region (Fig. 5j), indicating that the connection between SST trend in extratropical northern hemisphere and the trend of stratospheric wave activity is weak.

Figure 6 shows the first three EOF modes of September SST in SHtrop region during 2000-2017. The second mode (Fig. 6b) shows a great similarity to the spatial pattern of SST trend (Fig. 4b), and the corresponding PC2 time series also has a significant trend (slope=1.71, $p<0.01$). The correlation between PC2 and the Fz is significant ($r=-0.56$, $p=0.016$) and the correlation coefficient remains significant ($r=-0.46$, $p=0.065$) at the 90% confidence level when the value in 2002 is removed. This result suggests that the SST trend in SHtrop region is closely related to the recent weakening of stratospheric wave activities. The first EOF mode is similar to IPO (Fig. 6a) and its corresponding principal component is highly significantly correlated (r=-

https://doi.org/10.5194/acp-2021-395
Preprint. Discussion started: 1 June 2021

0.98, $p<0.01$) with the unfiltered IPO index. However, it shows no significant trend (Fig. 6d) and has no significant correlation (Fig. 6g) with stratospheric wave flux, implying that the linkage between the IPO phase change at around 2000 (e.g. Trenberth et al., 2013) and the weakening of Antarctic stratospheric wave activities is weak. The correlation between PC3 and Fz is also not significant (Fig. 6i). Therefore, it is possible that the combined effect of SST trend (the second EOF mode) in the tropical and extratropical southern hemisphere leads to the weakening of stratospheric wave activities in early austral spring since the early 2000s.

5. Simulated changes in Antarctic stratospheric wave activities forced by SST trends

The analysis in Section 4 suggests that the SST trend in SHtrop region may contribute to the weakening of the southern hemispheric stratospheric wave activities. Here, numerical experiments sstNH, sstSH, ssttrop and sstSHtrop forced by linear increments of SST in September during 2000-2017 (Fig. 7; more details can be found in Section 2) are conducted to verify the results discussed in Section 4.

Figure 8 shows the simulated response of 500 hPa geopotential height to SST changes in different regions. The climatological distributions of the wave-1 component (Figs. 8b, e, h, k) and the wave-2 component (Figs. 8c, f, i, l) from the simulations are consistent with that from reanalysis dataset (Figs. 4b, c), indicating that the model can well capture spatial distributions of the atmospheric waves. Note that the Fourier component (wave-1 and wave-2) anomalies simulated with SST changes in SH, TROP and SHtrop all are significant. They superpose on the corresponding climatological

https://doi.org/10.5194/acp-2021-395
Preprint. Discussion started: 1 June 2021

patterns in an out-of-phase style (Figs. 8e, f, h, i, k, l), indicating that the SST trends in SH, TROP and SHtrop lead to a weakening of tropospheric wave sources in the extratropical southern hemisphere. However, the 500 hPa geopotential height anomaly of the predominate wave-1 component in the extratropical southern hemisphere forced by the experiment with NH SST change is relatively weak (Fig. 8b). This feature suggests that the SST trend in extratropical northern hemisphere is incapable of inducing a robust response of tropospheric wave sources in the extratropical southern hemisphere.

Figure 9 shows the simulated responses of stratospheric wave activities in the southern hemisphere to SST changes in different regions. It is found that the experiments with SST changes in SH, TROP and SHtrop show significantly weakened stratospheric wave activities (Figs. 9d, g, j), which are mainly attributed to the responses of the wave-1 component (Figs. 9e, h, k). These results are consistent with the responses of tropospheric wave sources (Figs. 8d, e, g, h, j, k). However, there are no significant anomalies of stratospheric wave flux in the subpolar region as exhibited in Figures 9a and 9b, which is consistent with the response of corresponding tropospheric wave sources (Fig. 8a, b) and the weak correlation between Fz and PC time series of SST in NH region (Fig. 5i). It suggests that the response of southern hemisphere stratospheric wave activities to SST trend in NH region is weak.

Results of all these experiments are summarized and displayed in Figure 10, which is quantified by the frequency distribution of southern hemisphere stratospheric vertical wave flux derived from the 100 ensemble members of each experiment. Compared to

https://doi.org/10.5194/acp-2021-395
Preprint. Discussion started: 1 June 2021

the blue fitting curves, the red fitting curves shift to the left as shown in Figs. 10b, 10c and 10d, suggesting that the SST changes in SH, TROP and SHtrop regions weaken the upward propagation of stratospheric wave flux. The area-weighted anomalies of vertical E-P flux in the subpolar region of the southern hemisphere induced by SST changes in SH, TROP and SHtrop regions are -0.084×10^5 kg·s^{-2}, -0.12×10^5 kg·s^{-2} and -0.13×10^5 kg·s^{-2}, respectively. The sum of the anomalies forced by sstSH and ssttrop is not equal to the anomaly forced by sstSHtrop, which may be resulted from non-linear interactions between the responses of wave activities to SST trends in SH region and TROP region. The weakening of stratospheric wave activities forced by SST increment in the tropical region is more obvious and more significant than that in extratropical southern hemisphere (Figs. 10b, c, e), implying that the SST trend in the tropical region contributes more to the weakening of stratospheric wave activities since 2000. Meanwhile, it is apparent that the weakening of the southern hemisphere stratospheric wave activities forced by sstSHtrop is the most significant among all the sensitive experiments (Fig. 10e). The reduction of vertical E-P flux over (50°S-70°S, 200 hPa-10 hPa) forced by sstSHtrop is approximately 12%. These simulation results indicate that the weakening of the Antarctic stratospheric wave activities in September since 2000 is induced by the combined effects of SST trends in the tropical and extratropical southern hemisphere. It also explains why the independent correlation between Fz and PC obtained for SH or TROP region is not as significant as that between Fz and PC obtained for SHtrop region (Figs. 5g, h, j). Moreover, the mean linear increment of area-weighted vertical E-P flux from 200 hPa to 10 hPa over 70°S-50°S in September during

https://doi.org/10.5194/acp-2021-395
Preprint. Discussion started: 1 June 2021

2000-2017 derived from four reanalysis datasets is about -0.38×10^5 kg·s^{-2}. Therefore, the contribution of SST trend over 20°N-70°S (the SHtrop region) to the weakening of stratospheric activities is approximately 34%.

6. Conclusions and Discussion

This study analyzes the trend of Antarctic stratospheric planetary wave activities in early austral spring since the early 2000s based on various reanalysis datasets. Using the change-point method, we find that the Antarctic stratospheric wave activities in September have been weakening significantly since 2000, which means the intensified trend of wave activities noted in previous researches (Hu & Fu, 2009; Lin et al., 2009) are reversed after 2000 in early austral spring. Further analysis suggests that the weakening of stratospheric wave activities is related to the weakening of tropospheric wave sources in extratropical Southern Hemisphere, which is mainly contributed by the wave-1 component. Moreover, EOF analysis and correlation analysis indicate that the stratospheric wave activities in early austral spring during 2000-2017 are related to PC2 of SST over 20°N-70°S (i.e., the SHtrop region). The corresponding EOF2 mode also shows a great similarity to the spatial pattern of SST trend, suggesting that the weakening of stratospheric wave activities is connected to the trend of SST in SHtrop region. Meanwhile, the linkage between the SST trend in NH region and the weakening of stratospheric wave activities is weak. Finally, the model simulations support the conclusion that the SST changes in SHtrop region lead to the weakening of tropospheric wave sources and stratospheric wave activities. The contribution of SST trend in tropical region to the weakening of stratospheric wave activities is larger than that in

https://doi.org/10.5194/acp-2021-395
Preprint. Discussion started: 1 June 2021

the extratropical southern hemisphere. However, the response of tropospheric wave sources and stratospheric wave activities to SST trend in NH region is not significant. The contribution of SST trend over SHtrop region to the weakening of stratospheric wave activities is about 34%.

The question that remains answered is whether the ozone recovery trend also contributes to the weakening of stratospheric wave activities in September since the early 2000s. As described in Section 2, a control experiment (O3ctrl) forced by climatological ozone and a sensitive experiment forced by the linear increment of global ozone in September during 2001-2017 are conducted to address the above question. The pattern of ozone forcing field is similar to its trend pattern (Figs. S4c, d; Fig. S5). We choose the period of 2001-2017 because we notice that the ozone recovery trend derived from MERRA-2 in September with the beginning year of 2000 is not significant (Fig. S4a, b). Meanwhile, as the SSW in 2002 induces poleward transport of large amounts of ozone, the data in 2002 are removed when linear increments are calculated. Other details about these two experiments have been given in Section 2 and Table 2. The simulated results indicate that there is no significant response of wave flux (Fig. 11a, d) as well as its Fourier decomposed components (Fig. 11b, c) over southern hemisphere subpolar region in the stratosphere, suggesting that the prescribed ozone recovery is incapable of inducing the weakening of stratospheric wave activities.

Many researchers claimed that the climate transition around 2000 in the southern hemisphere is related to ozone depletion and recovery (e.g., Barnes et al., 2013; Banerjee et al., 2020). Note that there is no contradiction between our results and these

https://doi.org/10.5194/acp-2021-395
Preprint. Discussion started: 1 June 2021

previous studies. Firstly, the southern hemisphere tropospheric circulation (i.e., the SAM index, the tropospheric jet position and the Hadley cell edge) transition related to ozone depletion and recovery reported in these previous studies basically occurred in austral summer (e.g., Son et al., 2008; Thompson et al., 2011; Barnes et al., 2013; Banerjee et al., 2020). These tropospheric circulation transitions are induced by downward coupling of circulation anomalies in the stratosphere (e.g., Thompson et al., 2011) during October and November, when solar radiation covers the entire Antarctic and causes radiative heating effects. However, we focus on September in the present study. The Antarctic stratospheric circulation response to ozone variation in September is not as strong as that in October or November (e.g., Thompson et al., 2011, Fig. 1b, d) because solar radiation can only reach part of the Antarctic stratosphere during a majority period of September. This fact implies that the response of wave propagation environment in the Antarctic stratosphere to ozone trend is also not significant (Fig. S6). Secondly, the FWSC component used in this study is an atmospheric module with prescribed SST and gases. Therefore, the model results only indicate that the weakening of stratospheric wave activities can be attributed to SST trends, while the impact of ozone depletion and recovery trend in the tropics and mid-latitudes on the shift of SST trend pattern cannot be determined based on the model simulations. This is an issue beyond the scope of this study and further investigation is necessary using a fully coupled earth system model.

In addition, the reanalysis datasets show that the Brewer-Dobson circulation related to wave activities in the stratosphere weakened significantly in early austral spring during 2000-2017 (Fig. 12b), which is contrary to the intensified trend during 1980-2000 (Fig. 12a). The transition of BDC around 2000 is believed to be associated with ozone depletion and recovery (e.g., Polvani et al., 2017; Polvani et al., 2018). However, our modeling results suggest that the SST trend is responsible for the weakening of BDC in September since 2000 (Fig. 12d, e, f), The response of BDC to ozone recovery is not significant (Fig. 12c), especially for the branch near the Antarctic. These results indicate that the SST trend should be taken into consideration when exploring the mechanism for the climate transition in the southern hemispheric stratosphere around 2000.

Acknowledgements:

This work is supported by the National Natural Science Foundation of China (41630421 and 42075062). We thank Institute Pierre Simon Laplace (IPSL), NCEP and NCAR, National Aeronautics and Space Administration (NASA) and Japan Meteorological Agency (JMA) for providing ERA-Interim, NCEP-2, MERRA-2 and JRA-55 datasets. We thank National Oceanic and Atmospheric Administration (NOAA) for providing ERSST v5 dataset and IPO index. We also thank the scientific team at NCAR for providing CESM-1 model. Finally, we thank the computing support provided by the College of Atmospheric Sciences, Lanzhou University.

Reference

Andrews, D. G., Holton, J. R., & Leovy, C. B.: Middle atmosphere dynamics, (p. 489), San Diego,

https://doi.org/10.5194/acp-2021-395
Preprint. Discussion started: 1 June 2021

Calif: Academic Press Inc, 1987.

Angell, J. K., & Free, M.: Ground-based observations of the slowdown in ozone decline and onset of ozone increase, J. Geophys. Res., 114(D7), D07303, https://doi.org/10.1029/2008JD010860, 2009.

Brewer, A. W.: Evidence for a world circulation provided by the measurements of helium and water vapour distribution in the stratosphere, Q. J. Roy. Meteor. Soc., 75(326), 351-363, https://doi.org/10.1002/qj.49707532603, 1949.

Baldwin, M., P., Dunkerton, T. J.: Stratospheric harbingers of anomalous weather regimes, Science. https://doi.org/10.1126/science.1063315, 2001.

Baldwin, M., Hirooka, T., O'Neill, A., Yoden, S., Charlton, A. J., Hio, Y., & Yoden, S.: Major stratospheric warming in the Southern Hemisphere in 2002: Dynamical aspects of the ozone hole split, SPARC Newsletter, 20, 24–26, 2003.

Birner, T., & Bönisch, H.: Residual circulation trajectories and transit times into the extratropical lowermost stratosphere, Atmos. Chem. Phys., 11(2), 817–827, https://doi.org/10.5194/acp-11-817-2011, 2011.

Barnes, E. A., Barnes, N. W., Polvani, L. M.: Delayed southern hemisphere climate change induced by stratospheric ozone recovery, as projected by the cmip5 models, J. Climate, 27(2), 852-867, https://doi.org/10.1175/JCLI-D-13-00246.1, 2014

Bosilovich, M., Akella, S., Coy, L., Cullather, R., Draper, C., Gelaro, R. and Suarez, M.: MERRA-2: Initial Evaluation of the Climate, NASA Technical Report Series on Global Modeling and Data Assimilation, 43, 139, 2015.

Banerjee, A., Fyfe, J. C., Polvani, L. M., Waugh D., Chang K. L.: A pause in Southern Hemisphere

https://doi.org/10.5194/acp-2021-395
Preprint. Discussion started: 1 June 2021

circulation trends due to the Montreal Protocol, Nature, 579(7800), 544–548, https://doi.org/10.1038/s41586-020-2120-4, 2020.

Charney, J. G., & Drazin, P. G.: Propagation of planetary-scale disturbances from the lower into the upper atmosphere, J. Geophys. Res., 66(1), 83-109, https://doi.org/10.1029/JZ066i001p00083, 1961.

Dee, D. P., Uppala, S. M., Simmons, A. J., Berrisford, P., Poli, P., Kobayashi, S., et al.: The ERA-Interim reanalysis: Configuration and performance of the data assimilation system, Q. J. Roy. Meteor. Soc., 137(656), 553–597, https://doi.org/10.1002/qj.828, 2011.

Gillett, N. P., Allen, M. R., & Williams, K. D.: Modelling the atmospheric response to doubled CO2 and depleted stratospheric ozone using a stratosphere-resolving coupled GCM, Q. J. Roy. Meteor. Soc., 129(589), 947–966, https://doi.org/10.1256/qj.02.102, 2003.

Garcia, R. R., & Randel, W. J.: Acceleration of the brewer-dobson circulation due to increases in greenhouse gases, J. Atmos. Sci., 65(8), 2731-2739. https://doi.org/10.1175/2008JAS2712.1, 2008.

Gabriel, A., H. Körnich, Lossow, S., Peters, D. H. W., & Murtagh, D.: Zonal asymmetries in middle atmospheric ozone and water vapour derived from odin satellite data 2001–2010, Atmos. Chem. and Phys., 11(18), 9865-9885, https://doi.org/10.5194/acp-11-9865-2011, 2011.

Haynes, P. H., M. E. McIntyre, T. G. Shepherd, C. J. Marks, and K. P. Shine.: On the “Downward Control” of Extratropical Diabatic Circulations by Eddy-Induced Mean Zonal Forces, J. Atmos. Sci., 48(4), 651–678, https://doi.org/10.1175/1520-0469(1991)048<0651:OTCOED>2.0.CO;2, 1991.

Haigh, J. D., Blackburn, M., & Day, R.: The response of tropospheric circulation to perturbations in lower-stratospheric temperature, J. Climate, 18(17), 3672-3685. https://doi.org/10.1175/JCLI3472.1, 2005.

Holton, J.: An introduction to dynamic meteorology, Academic Pr., 2004.

Hu, Y., & Fu, Q.: Stratospheric warming in southern hemisphere high latitudes since 1979, Atmos. Chem. Phys., 9(13), 4329-4340, https://doi.org/10.5194/acp-9-4329-2009, 2009.

Hurwitz, M. M., Newman, P. A., Oman, L. D., & Molod, A. M.: Response of the antarctic stratosphere to two types of El niño events, J. Atmos. Sci., 68(4), 812-822. https://doi.org/10.1175/2011JAS3606.1, 2011.

Haarsma, R. J., & Selten, F.: Anthropogenic changes in the Walker circulation and their impact on the extra-tropical planetary wavestructure in the Northern Hemisphere, Clim. Dynam., 39(7-8), 1781–1799, https://doi.org/10.1007/s00382-012-1308-1, 2012.

Hu, D., Tian, W., Xie, F. Shu, J., Dhomse, S.: Effects of meridional sea surface temperature changes on stratospheric temperature and circulation, Adv. Atmos. Sci., 31, 888–900. https://doi.org/10.1007/s00376-013-3152-6, 2014.

Hu, D., Guan, Z., Tian, W., & Ren, R.: Recent strengthening of the stratospheric Arctic vortex response to warming in the central North Pacific, Nat. Commun., 9(1), 1697. https://doi.org/10.1038/s41467-018-04138-3, 2018.

Hu, D., Guo, Y., & Guan, Z.: Recent weakening in the stratospheric planetary wave intensity in early winter, Geophys. Res. Lett., 46(7), 3953-3962, https://doi.org/10.1029/2019GL082113, 2019.

Huang, B., Peter W. Thorne, et. al.: Extended Reconstructed Sea Surface Temperature version 5 (ERSSTv5), Upgrades, validations, and intercomparisons, J. Climate, 30(20), 8179-

https://doi.org/10.5194/acp-2021-395
Preprint. Discussion started: 1 June 2021

8205, https://doi.org/10.1175/JCLI-D-16-0836.1, 2017.

Ialongo, I., Sofieva, V., Kalakoski, N., Tamminen, J., & E. Kyrölä.: Ozone zonal asymmetry and planetary wave characterization during antarctic spring, Atmos. Chem. Phys., 12(5), 2603-2614, https://doi.org/10.5194/acp-12-2603-2012, 2012.

Kanamitsu, M., Ebisuzaki, W., Woollen, J., Yang, S. K., Hnilo, J. J., Fiorino, M., & Potter, G. L.: NCEP–DOE AMIP - II Reanalysis (R - 2), B. Am. Meteorol. Soc., 83(11), 1631–1644. https://doi.org/10.1175/BAMS-83-11-1631, 2002.

Kang, S. M. , Polvani, L. M. , Fyfe, J. C. , & Sigmond, M.: Impact of polar ozone depletion on subtropical precipitation, Science, 332(6032), 951-954, https://doi.org/10.1126/science.1202131, 2011.

Kravchenko, V. O., Evtushevsky, O. M., Grytsai, A. V., Klekociuk, A. R., Milinevsky, G. P., and Grytsai, Z. I.: Quasi-stationary planetary waves in late winter Antarctic stratosphere temperature as a possible indicator of spring total ozone, Atmos. Chem. Phys., 11(10), 28945–28967, https://doi.org/10.5194/acp-12-2865-2012, 2011.

Krzyścin J. W.: Onset of the total ozone increase based on statistical analyses of global ground-based data for the period 1964 – 2008, Int. J. Climatol., 32(2), 240-246, https://doi.org/10.1002/joc.2264, 2012.

Kim, B. M., Son, S. W., Min, S. K., Jeong, J. H., Kim, S. J., Zhang, X., Shim, T., Yoon, J. H.: Weakening of the stratospheric polar vortex by Arctic sea-ice loss, Nat. Commun., 5(1), 4646, https://doi.org/10.1038/ncomms5646, 2014.

Kobayashi, S., Y. Ota, Y. Harada, A. Ebita, M. Moriya, H. Onoda, K. Onogi, H. Kamahori, C. Kobayashi, H. Endo, K. Miyaoka, and K. Takahashi,: The JRA-55 Reanalysis: General

https://doi.org/10.5194/acp-2021-395
Preprint. Discussion started: 1 June 2021

specifications and basic characteristics, J. Meteorol. Soc. of Jpn., 93(1), 5-48, https://doi.org/10.2151/jmsj.2015-001, 2015.

Lin, P., Fu, Q., Solomon, S., & Wallace, J. M.: Temperature trend patterns in southern hemisphere high latitudes: novel indicators of stratospheric change, J. Climate, 22(23), 6325-6341. https://doi.org/10.1175/2009JCLI2971.1, 2009.

Li, S.: The influence of tropical indian ocean warming on the southern hemispheric stratospheric polar vortex, Sci. China. Ser. D., 52(3), 323–332, https://doi.org/10.1007/s11430-009-0029-8, 2009.

Lin, P., Fu, Q., & Hartmann, D.: Impact of tropical sst on stratospheric planetary waves in the southern hemisphere, J. Climate, 25(14), 5030-5046. https://doi.org/10.1175/JCLI-D-11-00378.1, 2012.

Li, Y., & Tian, W.: Different impact of central pacific and eastern pacific el nino on the duration of sudden stratospheric warming, Adv. Atmos. Sci., 34(06), 771-782. https://doi.org/10.1007/s00376-017-6286-0, 2017.

Li, Y., Tian, W., Xie, F., Wen, Z., Zhang, J., Hu, D., & Han, Y.: The connection between the second leading mode of the winter North Pacific sea surface temperature anomalies and stratospheric sudden warming events, Clim. Dynam., 51(1-2), 581 – 595. https://doi.org/10.1007/s00382-017-3942-0, 2018.

Lim, E. P., Hendon, H. H., Boschat, G. Hudson, D., Thompson, D. J., Dowdy, A., J., Arblaster, J. M.: Australian hot and dry extremes induced by weakenings of the stratospheric polar vortex, Nat. Geosci., 12, 896–901, https://doi.org/10.1038/s41561-019-0456-x, 2019.

Marsh, D. R., Mills, M. J., Kinnison, D. E., Lamarque, J. F., Calvo, N., & Polvani, L. M.: Climate

https://doi.org/10.5194/acp-2021-395
Preprint. Discussion started: 1 June 2021

change from 1850 to 2005 simulated in CESM1 (WACCM), J. Climate, 26(19), 7372-7391. https://doi.org/10.1175/JCLI-D-12-00558.1, 2013.

Nishii, K. and Nakamura, H.: Tropospheric influence on the diminished Antarctic ozone hole in September 2002, Geophys. Res. Lett., 31(16), L16103, https://doi.org/10.1029/2004GL019532, 2004.

Newman, P. A., & Nash, E. R.: The unusual Southern Hemisphere stratosphere winter of 2002, J. Atmos. Sci., 62(3), 614–628. https://doi.org/10.1175/JAS-3323.1, 2005.

Neale, R. B., Richter, J., Park, S., Lauritzen, Lauritzen, P. H., Vavrus, S. J., Rasch, P. J., & Zhang, M.:The mean climate of the community atmosphere model (cam4) in forced sst and fully coupled experiments, J. Climate, 26(14), 5150-5168, https://doi.org/10.1175/JCLI-D-12-00236.1, 2013.

Polvani, L. M., & Bellomo, K.: The key role of ozone depleting substances in weakening the walker circulation in the second half of the 20th century, J. Climate, 32(5), 1411-1418. https://doi.org/10.1175/JCLI-D-17-0906.1, 2013.

Polvani, L. M., Wang, L., Aquila, V., & Waugh, D. W.: The impact of ozone depleting substances on tropical upwelling, as revealed by the absence of lower stratospheric cooling since the late 1990s, J. Climate, 30(7), 2523-2534. https://doi.org/10.1175/JCLI-D-16-0532.1, 2017.

Polvani, L. M., Abalos, M., Garcia, R., Kinnison, D., & Randel, W. J.: Significant weakening of Brewer-Dobson circulation trends over the 21st century as a consequence of the Montreal Protocol, Geophys. Res. Lett., 45(1), 401–409, https://doi.org/10.1002/2017GL075345, 2018.

Randel, W. J., & Wu, F.: Cooling of the arctic and antarctic polar stratospheres due to ozone

https://doi.org/10.5194/acp-2021-395
Preprint. Discussion started: 1 June 2021

depletion, J. Climate, 12(5), 1467-1479. https://doi.org/10.1175/1520-0442(1999)012<1467:COTAAA>2.0.CO;2, 1999.

Solomon, S.: Stratospheric ozone depletion: a review of concepts and history, Rev. Geophys., 37(3), 275-316, https://doi.org/10.1029/1999RG900008, 1999.

Son, S. W., P. G. Edwin, K. H. Seo,: The impact of stratospheric ozone recovery on the Southern Hemisphere westerly jet, Science, 320(5882): 1486-1489, https://doi.org/10.1126/science.1155939, 2008.

Swart, N. C. & Fyfe, J. C.: Observed and simulated changes in the Southern Hemisphere surface westerly wind-stress, Geophys. Res. Lett. 39(16), L16711, https://doi.org/10.1029/2012GL052810, 2012.

Solomon, S., Ivy, D. J., Kinnison, D., Mills, M. J., Neely, R. R., & Schmidt, A.: Emergence of healing in the antarctic ozone layer, *Science*, 353(6296), 269-274, https://doi.org/10.1126/science.aae0061, 2016.

Son, S. W., Han, B. R., Garfinkel, C. I., Seo-Yeon, K., Rokjin, P., & Luke, A. N., et al.: Tropospheric jet response to antarctic ozone depletion: an update with chemistry-climate model initiative (CCMI) models, Environ. Res. Lett., 13(5), 054024-. https://doi.org/10.1088/1748-9326/aabf21, 2018.

Susan, E., S., Douglass, A. R., Damon, M. R.: Why do antarctic ozone recovery trends vary?, J. Geophys. Res.-Atmos., 124(15), 8837-8850. https://doi.org/10.1029/2019JD030996, 2019.

Shen, X., Wang, L., & Osprey, S.: The southern hemisphere sudden stratospheric warming of september 2019, Sci. Bull., 65(21), 1800-1802. https://doi.org/10.1016/j.scib.2020.06.028, 2020a

https://doi.org/10.5194/acp-2021-395
Preprint. Discussion started: 1 June 2021

Shen, X., Wang, L., & Osprey, S.: Tropospheric forcing of the 2019 antarctic sudden stratospheric warming, Geophys. Res. Lett., 47(20), e2020GLO89343, https://doi.org/10.1029/2020GL089343, 2020b.

Thompson, D., Solomon, S., Kushner, P. England, M., Grise, K. M., Karoly, D. J.: Signatures of the Antarctic ozone hole in Southern Hemisphere surface climate change, Nat. Geosci., 4, 741–749. https://doi.org/10.1038/ngeo1296, 2011.

Trenberth, K. E., & Fasullo, J. T.: An apparent hiatus in global warming?, Earth's Future, 1(1), 19–32, https://doi.org/10.1002/2013EF000165, 2013.

Tian, W., Li, Y., Xie, F., Zhang, J., Chipperfield, M., & Feng, W., Hu, Y., Zhao, S., Zhou, X., Zhang, Y. & Ma, X.: The relationship between lower-stratospheric ozone at southern high latitudes and sea surface temperature in the east Asian marginal seas in austral spring, Atmos. Chem. Phys., 17(11), 6705-6722. https://doi.org/10.5194/acp-17-6705-2017, 2017.

Wang, T., Tian, W., Zhang, J., Xie, F., Zhang, R., Huang, J. & Hu, D.: Connections between Spring Arctic Ozone and the Summer Circulation and Sea Surface Temperatures over the Western North Pacific, J. Climate, 33(7): 2907–2923, https://doi.org/10.1175/JCLI-D-19-0292.1, 2020.

WMO.: Scientific assessment of ozone depletion: 2010, World Meteorological Organization/United Nations Environment Programme Rep. 52, 516 pp, 2011.

WMO.: Antarctic ozone hole is smallest on record, World Meteorological Organization. Accessed October 2019 at https://public.wmo.int/en/media/news/antarctic-ozone-hole-smallest-record, 2019.

Xia, Y., Xu, W., Hu, Y., & Xie, F.: Southern-hemisphere high-latitude stratospheric warming

https://doi.org/10.5194/acp-2021-395
Preprint. Discussion started: 1 June 2021

revisit, Clim. Dynam., 54(3): 1671-1682. https://doi.org/10.1007/s00382-019-05083-7, 2020.

Xie, F., Zhang, J., Huang, Z., Lu, J., & Sun, C.: An estimate of the relative contributions of sea surface temperature variations in various regions to stratospheric change, J. Climate, 33(12), 4994-5011, https://doi.org/10.1175/JCLI-D-19-0743.1, 2020.

Yamazaki, Y., Matthias, V., Miyoshi, Y., Stolle, C., Siddiqui, T., Kervalishvili, G., et al.: September 2019 Antarctic sudden stratospheric warming: Quasi-6-day wave burst and ionospheric effects, Geophys. Res. Lett., 47(1), e2019GL086577. https://doi.org/10.1029/2019GL086577, 2020.

Zhang, J., Tian, W., Xie, F., Tian, H., Luo, J., Zhang, J., Liu, W., Dhomse, S.: Climate warming and decreasing total column ozone over the tibetan plateau during winter and spring, Tellus B., 66(1), https://doi.org/10.3402/tellusb.v66.23415, 2014.

Zhang, J., Tian, W. , Chipperfield, M. P. , Xie, F. , & Huang, J.: Persistent shift of the arctic polar vortex towards the eurasian continent in recent decades, Nat. Clim. Change. 6, 1094–1099. https://doi.org/10.1038/nclimate3136, 2016.

Zhang, P., Wu, Y. & Smith, K. L.: Prolonged effect of the stratospheric pathway in linking Barents–Kara Sea sea ice variability to the midlatitude circulation in a simplified model, Clim. Dynam. 50(17), 527–539. https://doi.org/10.1007/s00382-017-3624-y, 2018.

Zhang, J., Tian, W., Xie, F., Sang, W., Guo, D., Chipperfield, M., Feng, W., Hu, D.: Zonally asymmetric trends of winter total column ozone in the northern middle latitudes, Clim. Dynam., 52(7-8), 4483-4500, https://doi.org/10.1007/s00382-018-4393-y, 2019a.

Zhang, R., Tian, W., Zhang, J., Huang, J., & Xu, M.: The corresponding tropospheric environments

https://doi.org/10.5194/acp-2021-395
Preprint. Discussion started: 1 June 2021

during downward-extending and nondownward-extending events of stratospheric northern annular mode anomalies, J. Climate, 32(6), 1857-1873, https://doi.org/10.1175/JCLI-D-18-0574.1, 2019b.

Table 1. Configurations of experiments for SST trends.

Experiments	Descriptions
sstctrl	Control run. Seasonal cycle of monthly mean global SST data over 1980-2000 is derived from the ERSST v5 dataset. Fixed values of ozone greenhouse gases and aerosol fields in 2000 are used.
sstNH	As in sstctrl, but with linear increments of SST in September over 2000-2017 in NH (20°N-70°N). The applied global SST anomalies are shown in Fig. 7a.
sstSH	As in sstctrl, but with linear increments of SST in September over 2000-2017 in SH (20°S-70°S). The applied global SST anomalies are shown in Fig. 7b.
ssttrop	As in sstctrl, but with linear increments of SST in September over 2000-2017 in the tropics (20°S-20°N). The applied global SST anomalies are shown in Fig. 7c.
sstSHtrop	As in sstctrl, but with linear increments of SST in September over 2000-2017 in SHtrop (20°N-70°S). The applied global SST anomalies are shown in Fig. 7d.

Table 2. Configurations of experiments for the ozone recovery trend.

Experiments	Descriptions

O3ctrl	Control run. The seasonal cycle of monthly averaged global SST data over 1980-2000 is derived from ERSST v5 dataset. The seasonal cycle of monthly mean three-dimensional global ozone over 1980-2000 is derived from MERRA-2 dataset. The GHGs and aerosol fields are specified to be fixed values in 2000.
O3sen	As in O3ctrl, but superposed with linear increments of global ozone in September over 2001-2017. The ozone data in 2002 are removed when the linear increments are calculated. The applied ozone anomalies in Southern Hemisphere are shown in Fig. S5.

Table 3. Correlations of stratospheric vertical wave flux time series (area-weighted from 100 hPa to 30 hPa over 70°S-50°S) between different reanalysis dataset.

	ERA-Interim	JRA-55	MERRA-2	NCEP-2
ERA-Interim	1.00 (p=0.00)	0.99 (p<0.01)	0.98 (p<0.01)	0.93 (p<0.01)
JRA-55		1.00 (p=0.00)	0.98 (p<0.01)	0.93 (p<0.01)
MERRA-2			1.00 (p=0.00)	0.94 (p<0.01)
NCEP-2				1.00 (p=0.00)

Figure captions:

FIG. 1. Trends of southern hemisphere (a, d) stratospheric E-P flux (arrows, units of horizontal and vertical components are 10^5 and 10^3 $kg{\cdot}s^{-2}$ per year, respectively) and its divergence (shadings) with their (b, e) wave-1 components and (c, f) wave-2 components over (a, b, c) 1980-2000 and (d, e, f) 2000-2017 in September derived from MERRA-2 dataset. The stippled regions indicate the trend of E-P flux divergence significant at/above the 90% confidence level. The green contours from outside to inside (corresponding to p=0.1, 0.05) indicate the trend of vertical E-P flux significant

https://doi.org/10.5194/acp-2021-395
Preprint. Discussion started: 1 June 2021

at the 90% and 95% confidence level, respectively.

FIG. 2. (a) The mean time series (solid line) and piecewise (during 1980-2000 and 2000-2018) linear regressions (dashed lines) of vertical E-P flux area-weighted from 100 hPa to 30 hPa over 70°S-50°S in September during 1980-2018 derived from ERA-Interim (yellow), MERRA-2 (blue), JRA-55 (red) and NCEP-2 (green). Figure (b) is the same as Figure (a), except for that the data in 2002 are removed. (c, d, e, f) The trends (dots) and uncertainties (error bars) calculated during various periods using the change-point method with different beginning and ending years (titles). Circles and squares in Figures (c, d, e, f) represent positive trends from beginning years to change-point years (x-axes) and negative trends from change-point years to ending years, respectively. Different colors of dots and error bars in Figures (c, d, e, f) correspond to colors in Figure (a), which represent trends and uncertainties derived from different datasets. The long and short error bars in same color reflect the 95% and 90% confidence intervals calculated by two-tailed t test. The error bar is omitted when the significance of trend is lower than corresponding confidence level. Negative trends and corresponding uncertainties with the beginning change-point years after 2005 are also omitted, since the trend value shows large fluctuation with shortening of time series. Figures (g, h, i, j) are the same as Figures (c, d, e, f), except that the data in 2002 are removed when calculating trends and uncertainties.

FIG. 3. Trends (shadings) and climatological distributions (contours with an interval of 20 gpm, positive and negative values are depicted by solid and dashed lines respectively, zeroes are depicted by thick solid lines) of southern hemispheric (a) 500

https://doi.org/10.5194/acp-2021-395
Preprint. Discussion started: 1 June 2021

hPa geopotential height zonal deviations with their (b) wave-1 component and (c) wave-2 component in September during 2000−2017 derived from MERRA-2 dataset. Trends of southern hemispheric (d) tropospheric E-P flux (arrows, units of horizontal and vertical components are 3×10^5 and 3×10^3 kg s^{-2} per year, respectively) and its vertical component (shading) with their (e) wave-1 component and (f) wave-2 component in September during 2000−2017 derived from MERRA-2 dataset. The stippled regions represent the trend significant at/above the 90% confidence level.

FIG. 4. Trends of SST in September over (a) 1980-2000 and (b) 2000-2017 derived from ERSST v5 dataset. The stippled regions represent the trends significant at/above the 90% confidence level.

FIG. 5. Trend significance of the first three SST principal components (PCs) in (a) the extratropical southern hemisphere (SH, 70°S-20°S), (b) the tropics (TROP, 20°S-20°N), (c) the extratropical northern hemisphere (NH, 20°N-70°N), (d) the extratropical southern hemisphere and the tropics (SHtrop, 70°S-20°N), (e) the extratropical northern hemisphere and the tropics (NHtrop, 20°S-70°N), (f) the globe (70°S-70°N) and the corresponding (g, h, i, j, k, l) correlation significances between them and vertical E-P flux (Fz, area-weighted from 100 hPa to 30 hPa over 70°S-50°S) during different beginning years (x-axes) and ending years (y-axes). The red and blue dots indicate positive and negative trend or correlation coefficient are significant, respectively. The black dots indicate the trends or correlation coefficients are not significant. The stars indicate that the trends and the corresponding correlation coefficients are both significant. Each panel is divided into three regions from bottom to top, corresponding

https://doi.org/10.5194/acp-2021-395
Preprint. Discussion started: 1 June 2021

to the first, the second and the third principal components, respectively. The criterion to distinguish whether the trends and correlations are significant or not is the 90% confidence level.

FIG. 6. (a, b, c) The first three EOF patterns of SST in SHtrop region. (d, e, f) The original time series of the first three principle components (PCs, blue solid lines correspond to left inverted y-axes) and stratospheric vertical E-P flux (Fz, area-weighted from 100 hPa to 30 hPa over 70°S-50°S, red solid lines correspond to right y-axes) in September during 2000-2017. The blue and red dashed lines in (d, e, f) represent the linear regressions of PC time series and Fz time series, respectively. The meaning of (g, h, i) are the same as (d, e, f) correspondingly, except the detrended time series. The unbracketed and bracketed numbers in (g, h, i) represent the correlation coefficients between detrended PC time series and Fz time series and the corresponding p values calculated by two-tailed t test, respectively.

FIG. 7. Differences in SST forcing field between sensitive experiments ((a) sstNH; (b) sstSH; (c) ssttrop; (d) sstSHtrop) and the control experiment (sstctrl).

FIG. 8. Differences (shadings) of (a, d, g, j) 500 hPa geopotential height zonal deviations with their (b, e, h, k) wave-1 component and (c, f, i, l) wave-2 component between sensitive experiments ((a, b, c) sstNH; (d, e, f) sstSH; (g, h, i) ssttrop; (j, k, l) sstSHtrop) and the control experiment (sstctrl). The mean distributions (contours with an interval of 20 gpm, positive and negative values are depicted by solid and dashed lines respectively, zeroes are depicted by thick solid lines) of them are derived from the control experiment. The stippled regions represent the mean difference significant

https://doi.org/10.5194/acp-2021-395
Preprint. Discussion started: 1 June 2021

Atmospheric Chemistry and Physics
Open Access
Discussions

at/above the 90% confidence level.

FIG. 9. Differences of (a, d, g, j) stratospheric E-P flux (arrows, units in horizontal and vertical components are 0.05×10^7 and 0.05×10^5 $kg\cdot s^{-2}$, respectively) and its divergence (shadings) with their (b, e, h, k) wave-1 component and (c, f, i, l) wave-2 component between sensitive experiments ((a, b, c) sstNH; (d, e, f) sstSH; (g, h, i) ssttrop; (j, k, l) sstSHtrop) and the control experiment (sstctrl). The stippled regions represent the mean differences of E-P flux divergence significant at/above the 90% confidence level. The green contours from outside to inside (corresponding to p=0.1, 0.05) represent the mean differences of vertical E-P flux significant at the 90% and 95% confidence levels, respectively.

FIG. 10. (a, b, c, d) Frequency distributions (pillars, blue for control experiment and orange for sensitive experiments) of vertical E-P flux (Fz, area-weighted from 200 hPa to 10 hPa over 70°S-50°S) and its 5-point low-pass filtered fitting curves (solid lines, blue for control experiment and red for sensitive experiments) derived from 100 ensemble members of the control experiment (sstctrl) and sensitive experiments ((a) sstNH; (b) sstSH; (c) ssttrop; (d) sstSHtrop), respectively. (e) Mean differences (grey pillars) and corresponding uncertainties (error bars) of Fz between sensitive experiments and the control experiment. The blue and red error bars reflect the 90% and 95% confidence levels calculated by two-tailed t test, respectively. The error bar is omitted when the significance of mean difference is lower than the corresponding confidence level.

FIG. 11. Differences of (a) stratospheric E-P flux (arrows, units in horizontal and

https://doi.org/10.5194/acp-2021-395
Preprint. Discussion started: 1 June 2021

Atmospheric Chemistry and Physics Discussions
Open Access

vertical components are 0.02×10^{7} and 0.05×10^{5} $kg\cdot s^{-2}$, respectively) and its divergence (shadings) with their (b) wave-1 component and (c) wave-2 component between the sensitive experiment (O3sen) and the control experiment (O3ctrl). The stippled regions represent the mean differences of E-P flux divergence significant at/above the 90% confidence level. The green contours from outside to inside (corresponding to p=0.1, 0.05) represent the mean differences of vertical E-P flux significant at the 90% and 95% confidence levels, respectively. (d) Frequency distributions (pillars, blue for O3ctrl and orange for O3sen) of vertical E-P flux (Fz, area-weighted from 200 hPa to 10 hPa over 70°S-50°S) and it 5-point low-pass filtered fitting curves (solid lines, blue for O3ctrl and red for O3sen) derived from 100 ensemble members.

FIG. 12. (a) Trends of southern hemispheric Brewer-Dobson circulation (arrows, units in horizontal and vertical components are 0.2×10^{-2} and 0.2×10^{-4} $m\cdot s^{-1}$ per year, respectively) and its stream function (shadings) in September during (a) 1980-2000 and (b) 2000-2017 derived from MERRA-2 dataset. Data in 2002 are removed when trends are calculated in Figure (b). (c) Differences of Brewer-Dobson circulation (arrows, units in horizontal and vertical components are 10^{-2} and 10^{-4} $m\cdot s^{-1}$, respectively) and its stream function (shadings) between the O3ctrl and O3sen. (d, e, f) Differences of Brewer-Dobson circulation and its stream function between the control experiment (sstctrl) and various sensitive experiments ((d) sstSH; (e) ssttrop; (f) sstSHtrop) with SST changes. The stippled regions represent the trends or differences of the stream function significant at/above the 90% confidence level. The green contours from outside to inside (corresponding to p=0.1, 0.05) represent the trends or differences of

https://doi.org/10.5194/acp-2021-395
Preprint. Discussion started: 1 June 2021

Atmospheric Chemistry and Physics
Discussions

the vertical components significant at the 90% and 95% confidence levels, respectively.

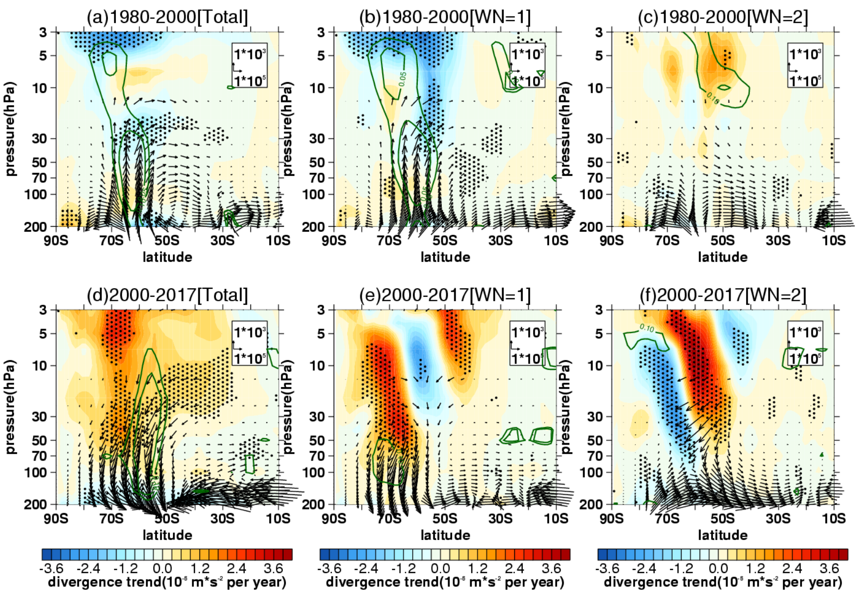

FIG. 1. Trends of southern hemisphere (a, d) stratospheric E-P flux (arrows, units of horizontal and vertical components are 10^5 and 10^3 kg·s^{-2} per year, respectively) and its divergence (shadings) with their (b, e) wave-1 components and (c, f) wave-2 components over (a, b, c) 1980-2000 and (d, e, f) 2000-2017 in September derived from MERRA-2 dataset. The stippled regions indicate the trend of E-P flux divergence significant at/above the 90% confidence level. The green contours from outside to inside (corresponding to p=0.1, 0.05) indicate the trend of vertical E-P flux significant at the 90% and 95% confidence level, respectively.

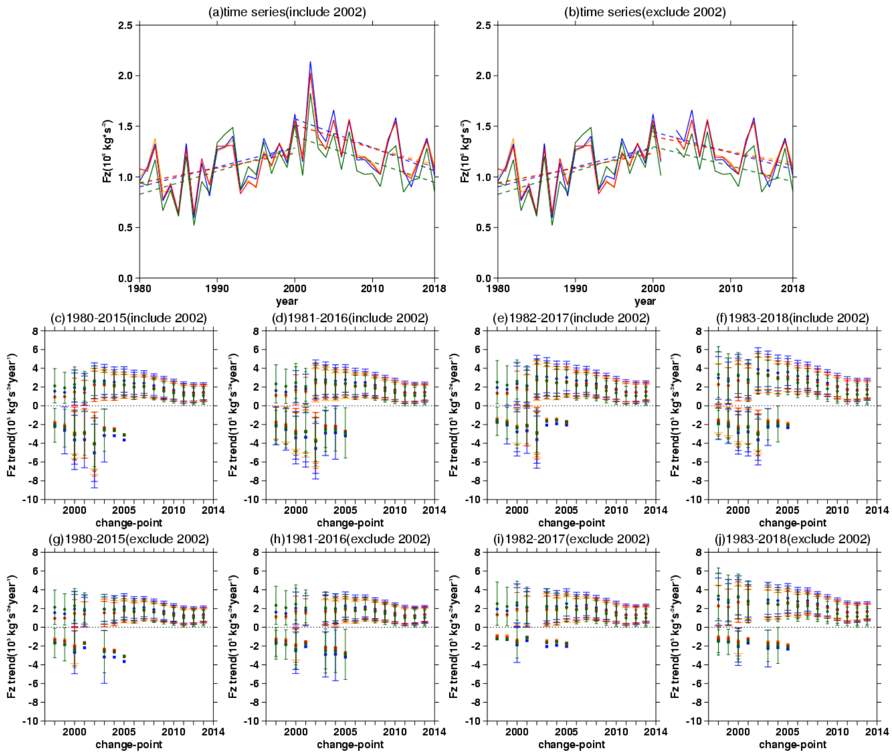

FIG. 2. (a) The mean time series (solid line) and piecewise (during 1980-2000 and 2000-2018) linear regressions (dashed lines) of vertical E-P flux area-weighted from 100 hPa to 30 hPa over 70°S-50°S in September during 1980-2018 derived from ERA-Interim (yellow), MERRA-2 (blue), JRA-55 (red) and NCEP-2 (green). Figure (b) is the same as Figure (a), except for that the data in 2002 are removed. (c, d, e, f) The trends (dots) and uncertainties (error bars) calculated during various periods using the change-point method with different beginning and ending years (titles). Circles and squares in Figures (c, d, e, f) represent positive trends from beginning years to change-point years (x-axes) and negative trends from change-point years to ending years, respectively. Different colors of dots and error bars in Figures (c, d, e, f) correspond to colors in Figure (a), which represent trends and uncertainties derived from different

https://doi.org/10.5194/acp-2021-395
Preprint. Discussion started: 1 June 2021

datasets. The long and short error bars in same color reflect the 95% and 90% confidence intervals calculated by two-tailed t test. The error bar is omitted when the significance of trend is lower than corresponding confidence level. Negative trends and corresponding uncertainties with the beginning change-point years after 2005 are also omitted, since the trend value shows large fluctuation with shortening of time series. Figures (g, h, i, j) are the same as Figures (c, d, e, f), except that the data in 2002 are removed when calculating trends and uncertainties.

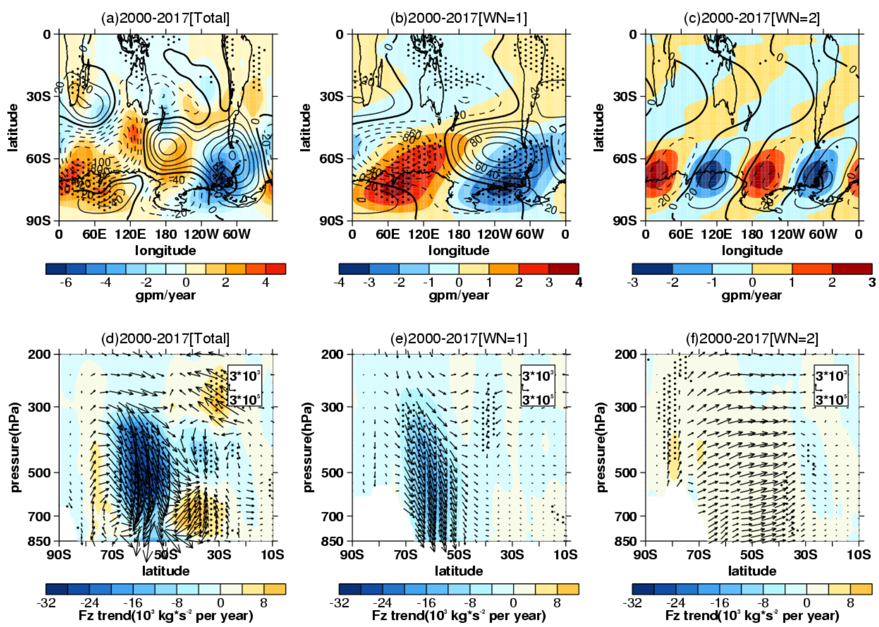

FIG. 3. Trends (shadings) and climatological distributions (contours with an interval of 20 gpm, positive and negative values are depicted by solid and dashed lines respectively, zeroes are depicted by thick solid lines) of southern hemispheric (a) 500 hPa geopotential height zonal deviations with their (b) wave-1 component and (c) wave-2 component in September during 2000−2017 derived from MERRA-2 dataset. Trends of southern hemispheric (d) tropospheric E-P flux (arrows, units of horizontal

https://doi.org/10.5194/acp-2021-395
Preprint. Discussion started: 1 June 2021

and vertical components are 3×10^5 and 3×10^3 kg s^{-2} per year, respectively) and its vertical component (shading) with their (e) wave-1 component and (f) wave-2 component in September during 2000−2017 derived from MERRA-2 dataset. The stippled regions represent the trend significant at/above the 90% confidence level.

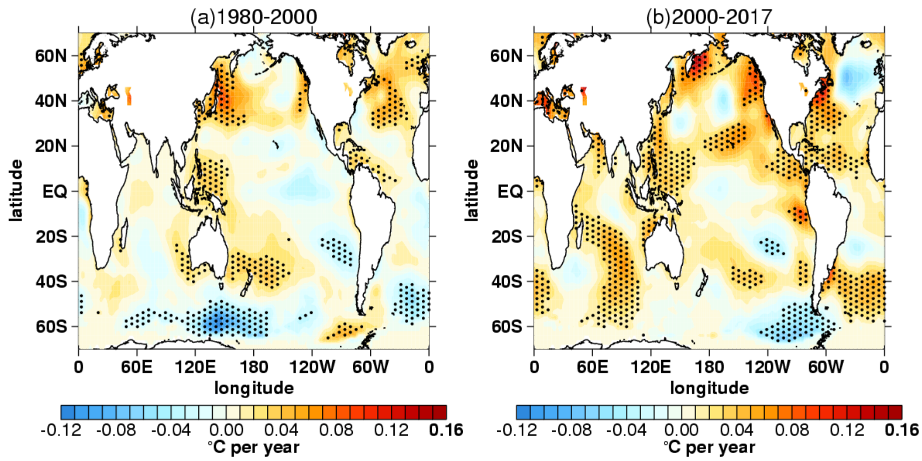

FIG. 4. Trends of SST in September over (a) 1980-2000 and (b) 2000-2017 derived from ERSST v5 dataset. The stippled regions represent the trends significant at/above the 90% confidence level.

https://doi.org/10.5194/acp-2021-395
Preprint. Discussion started: 1 June 2021

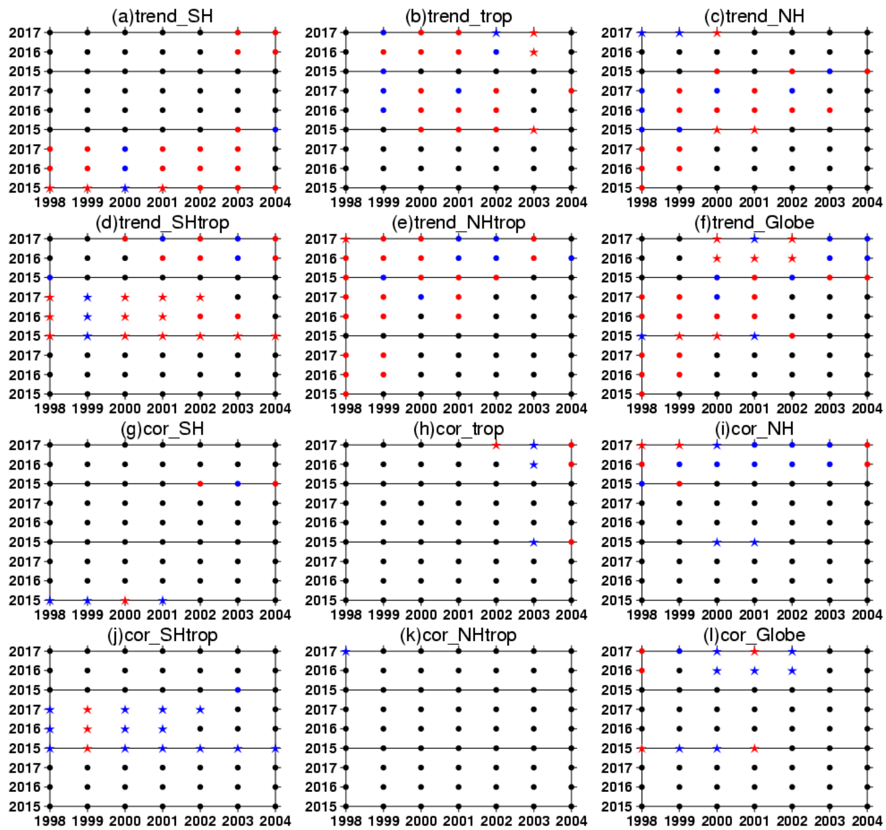

FIG. 5. Trend significance of the first three SST principal components (PCs) in (a) the extratropical southern hemisphere (SH, 70°S-20°S), (b) the tropics (TROP, 20°S-20°N), (c) the extratropical northern hemisphere (NH, 20°N-70°N), (d) the extratropical southern hemisphere and the tropics (SHtrop, 70°S-20°N), (e) the extratropical northern hemisphere and the tropics (NHtrop, 20°S-70°N), (f) the globe (70°S-70°N) and the corresponding (g, h, i, j, k, l) correlation significances between them and vertical E-P flux (Fz, area-weighted from 100 hPa to 30 hPa over 70°S-50°S) during different beginning years (x-axes) and ending years (y-axes). The red and blue dots indicate positive and negative trend or correlation coefficient are significant, respectively. The black dots indicate the trends or correlation coefficients are not significant. The stars

https://doi.org/10.5194/acp-2021-395
Preprint. Discussion started: 1 June 2021

Atmospheric Chemistry and Physics
Discussions

indicate that the trends and the corresponding correlation coefficients are both significant. Each panel is divided into three regions from bottom to top, corresponding to the first, the second and the third principal components, respectively. The criterion to distinguish whether the trends and correlations are significant or not is the 90% confidence level.

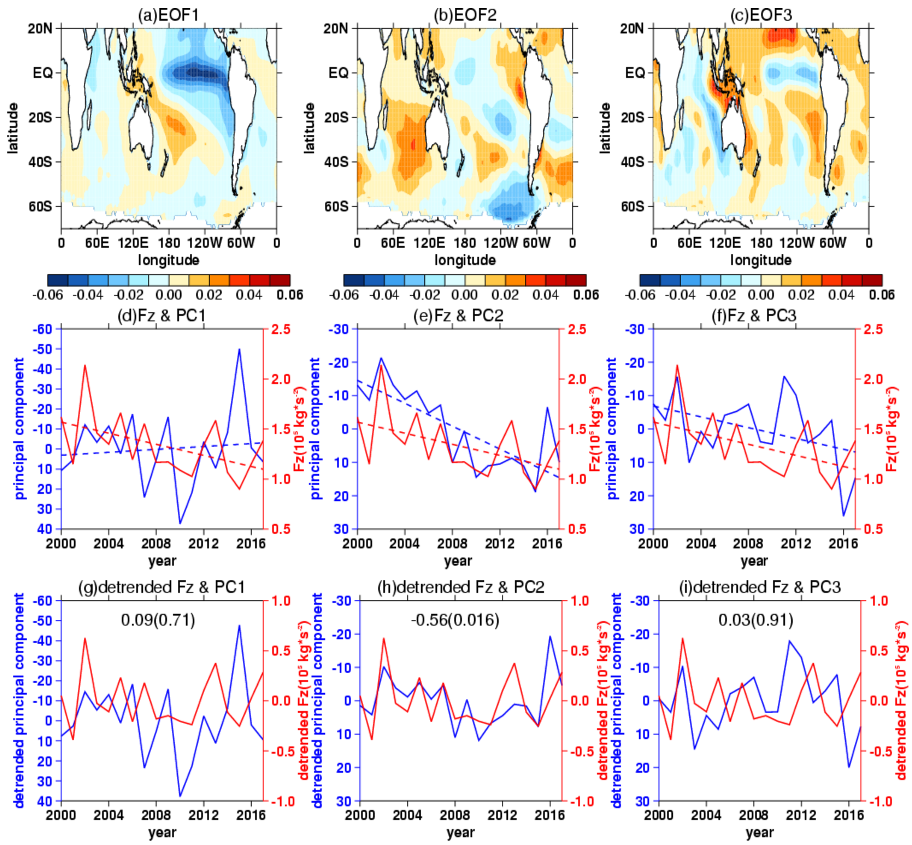

FIG. 6. (a, b, c) The first three EOF patterns of SST in SHtrop region. (d, e, f) The original time series of the first three principle components (PCs, blue solid lines correspond to left inverted y-axes) and stratospheric vertical E-P flux (Fz, area-weighted from 100 hPa to 30 hPa over 70°S-50°S, red solid lines correspond to right y-axes) in September during 2000-2017. The blue and red dashed lines in (d, e, f)

https://doi.org/10.5194/acp-2021-395
Preprint. Discussion started: 1 June 2021

Atmospheric Chemistry and Physics
Discussions

represent the linear regressions of PC time series and Fz time series, respectively. The meaning of (g, h, i) are the same as (d, e, f) correspondingly, except the detrended time series. The unbracketed and bracketed numbers in (g, h, i) represent the correlation coefficients between detrended PC time series and Fz time series and the corresponding p values calculated by two-tailed t test, respectively.

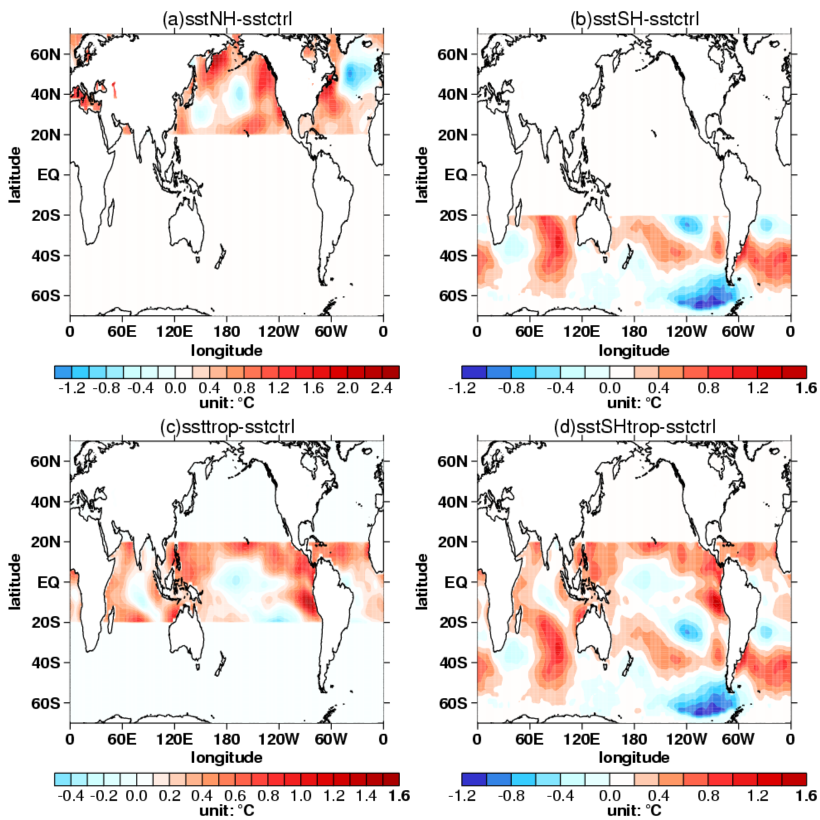

FIG. 7. Differences in SST forcing field between sensitive experiments ((a) sstNH; (b) sstSH; (c) ssttrop; (d) sstSHtrop) and the control experiment (sstctrl).

https://doi.org/10.5194/acp-2021-395
Preprint. Discussion started: 1 June 2021

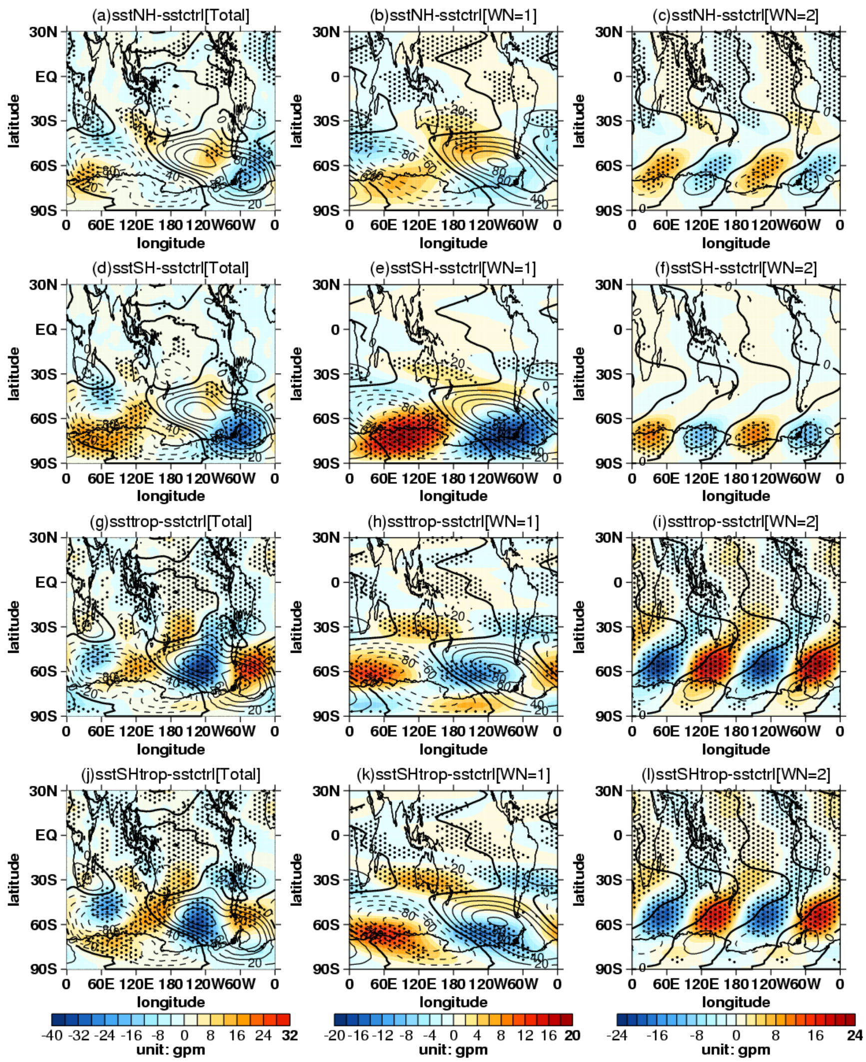

FIG. 8. Differences (shadings) of (a, d, g, j) 500 hPa geopotential height zonal deviations with their (b, e, h, k) wave-1 component and (c, f, i, l) wave-2 component between sensitive experiments ((a, b, c) sstNH; (d, e, f) sstSH; (g, h, i) ssttrop; (j, k, l) sstSHtrop) and the control experiment (sstctrl). The mean distributions (contours with an interval of 20 gpm, positive and negative values are depicted by solid and dashed lines respectively, zeroes are depicted by thick solid lines) of them are derived from the

https://doi.org/10.5194/acp-2021-395
Preprint. Discussion started: 1 June 2021

Atmospheric Chemistry and Physics Discussions

control experiment. The stippled regions represent the mean difference significant at/above the 90% confidence level.

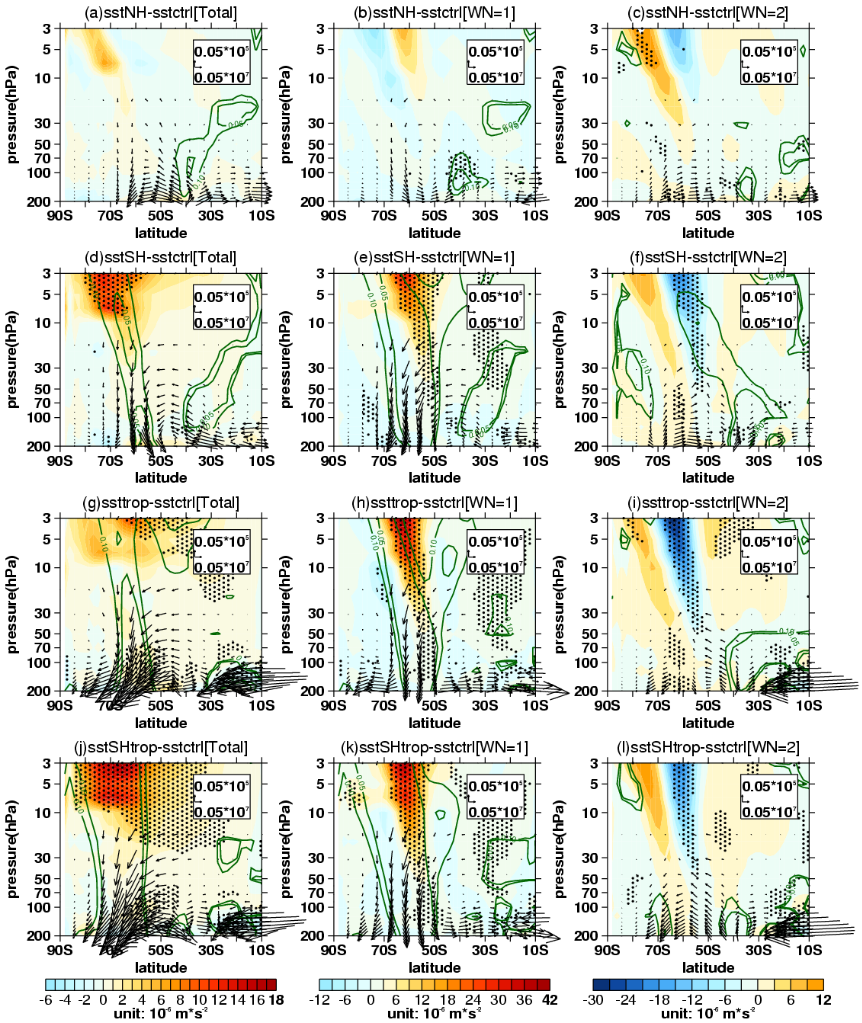

FIG. 9. Differences of (a, d, g, j) stratospheric E-P flux (arrows, units in horizontal and vertical components are 0.05×10^7 and 0.05×10^5 kg·s^{-2}, respectively) and its divergence (shadings) with their (b, e, h, k) wave-1 component and (c, f, i, l) wave-2 component between sensitive experiments ((a, b, c) sstNH; (d, e, f) sstSH; (g, h, i) ssttrop; (j, k, l) sstSHtrop) and the control experiment (sstctrl). The stippled regions represent the mean

https://doi.org/10.5194/acp-2021-395
Preprint. Discussion started: 1 June 2021

differences of E-P flux divergence significant at/above the 90% confidence level. The green contours from outside to inside (corresponding to p=0.1, 0.05) represent the mean differences of vertical E-P flux significant at the 90% and 95% confidence levels, respectively.

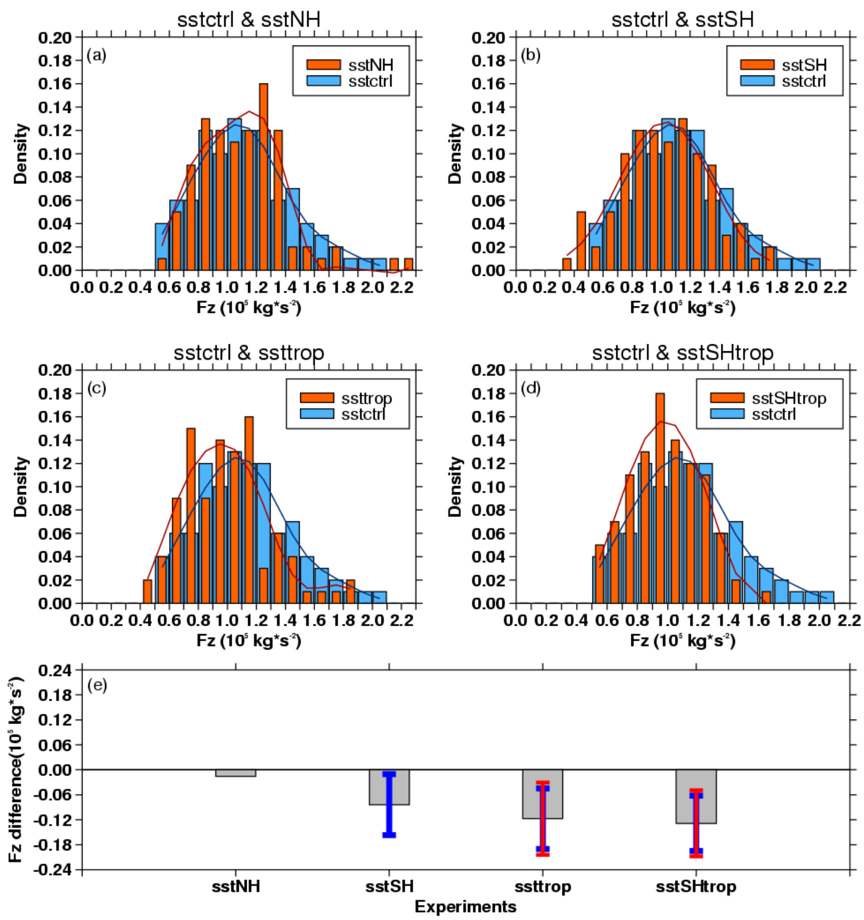

FIG. 10. (a, b, c, d) Frequency distributions (pillars, blue for control experiment and orange for sensitive experiments) of vertical E-P flux (Fz, area-weighted from 200 hPa to 10 hPa over 70°S-50°S) and its 5-point low-pass filtered fitting curves (solid lines, blue for control experiment and red for sensitive experiments) derived from 100

https://doi.org/10.5194/acp-2021-395
Preprint. Discussion started: 1 June 2021

Atmospheric Chemistry and Physics Discussions

ensemble members of the control experiment (sstctrl) and sensitive experiments ((a) sstNH; (b) sstSH; (c) ssttrop; (d) sstSHtrop), respectively. (e) Mean differences (grey pillars) and corresponding uncertainties (error bars) of Fz between sensitive experiments and the control experiment. The blue and red error bars reflect the 90% and 95% confidence levels calculated by two-tailed t test, respectively. The error bar is omitted when the significance of mean difference is lower than the corresponding confidence level.

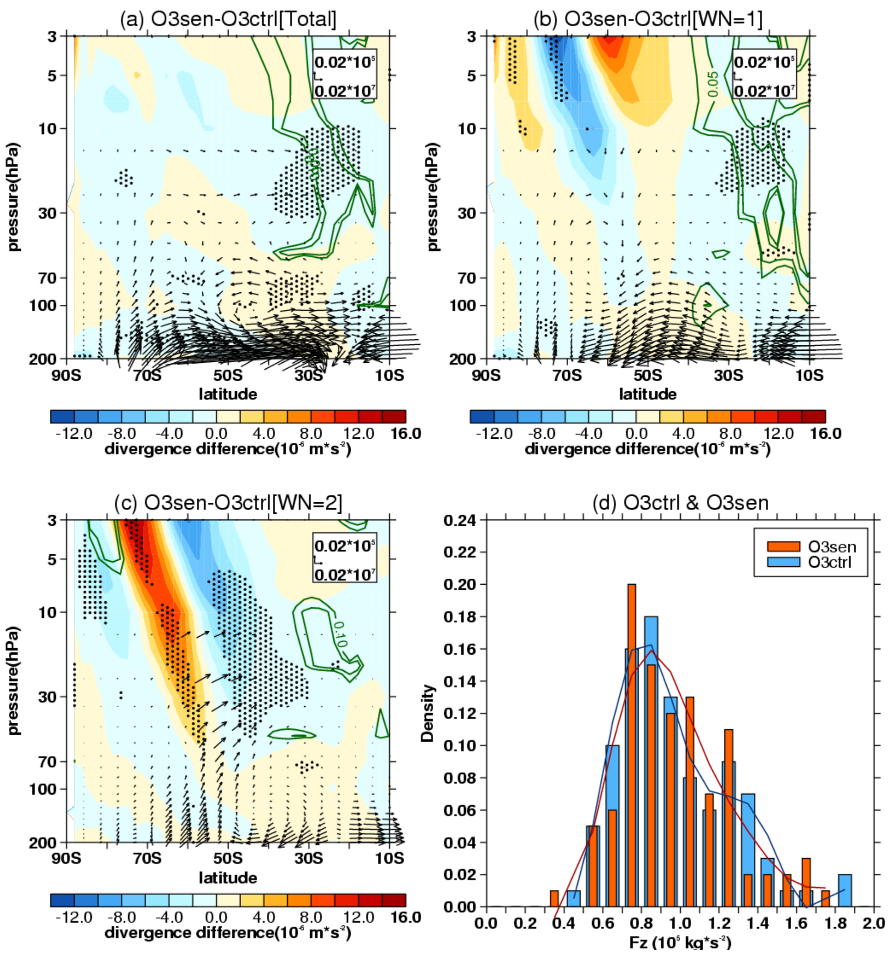

FIG. 11. Differences of (a) stratospheric E-P flux (arrows, units in horizontal and

https://doi.org/10.5194/acp-2021-395
Preprint. Discussion started: 1 June 2021

vertical components are 0.02×10^7 and 0.05×10^5 $kg\cdot s^{-2}$, respectively) and its divergence (shadings) with their (b) wave-1 component and (c) wave-2 component between the sensitive experiment (O3sen) and the control experiment (O3ctrl). The stippled regions represent the mean differences of E-P flux divergence significant at/above the 90% confidence level. The green contours from outside to inside (corresponding to p=0.1, 0.05) represent the mean differences of vertical E-P flux significant at the 90% and 95% confidence levels, respectively. (d) Frequency distributions (pillars, blue for O3ctrl and orange for O3sen) of vertical E-P flux (Fz, area-weighted from 200 hPa to 10 hPa over 70°S-50°S) and it 5-point low-pass filtered fitting curves (solid lines, blue for O3ctrl and red for O3sen) derived from 100 ensemble members.

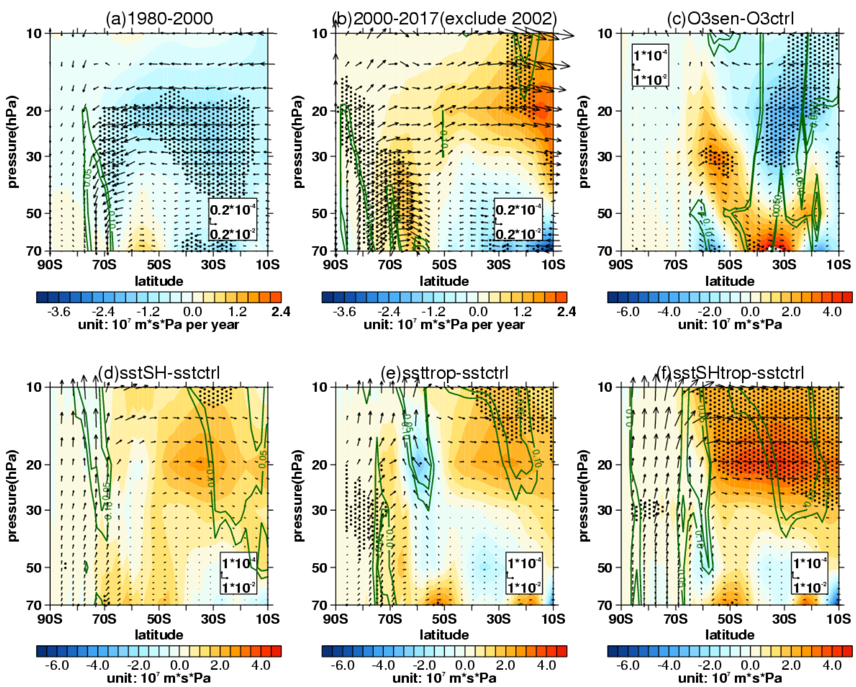

FIG. 12. (a) Trends of southern hemispheric Brewer-Dobson circulation (arrows, units in horizontal and vertical components are 0.2×10^{-2} and 0.2×10^{-4} $m\cdot s^{-1}$ per year,

https://doi.org/10.5194/acp-2021-395
Preprint. Discussion started: 1 June 2021

respectively) and its stream function (shadings) in September during (a) 1980-2000 and (b) 2000-2017 derived from MERRA-2 dataset. Data in 2002 are removed when trends are calculated in Figure (b). (c) Differences of Brewer-Dobson circulation (arrows, units in horizontal and vertical components are 10^{-2} and 10^{-4} $m \cdot s^{-1}$, respectively) and its stream function (shadings) between the O3ctrl and O3sen. (d, e, f) Differences of Brewer-Dobson circulation and its stream function between the control experiment (sstctrl) and various sensitive experiments ((d) sstSH; (e) ssttrop; (f) sstSHtrop) with SST changes. The stippled regions represent the trends or differences of the stream function significant at/above the 90% confidence level. The green contours from outside to inside (corresponding to p=0.1, 0.05) represent the trends or differences of the vertical components significant at the 90% and 95% confidence levels, respectively.